Earth-Science Reviews 269 (2025) 105197

Contents lists available at ScienceDirect

Earth-Science Reviews

journal homepage: www.elsevier.com/locate/earscirev

Review Article

Characteristics, genesis, and significance of laumontite in sedimentary rocks of non-marine petroliferous basins in China

Huan Tong [a,b], Shifa Zhu [a,b,*], Hanyun Tian [a,b], Hang Cui [a,b], Zhuoya Si [a,b], Yan Chen [a,b], Xincai You [c], Zhensheng Shi [d], Jianqin Xue [a,b,e]

[a] State Key Laboratory of Petroleum Resources and Engineering, China University of Petroleum (Beijing), Beijing 102249, China
[b] College of Geosciences, China University of Petroleum (Beijing), Beijing 102249, China
[c] Research Institute of Exploration & Development, PetroChina Xinjiang Oilfield Company, Karamay 834000, China
[d] Research Institute of Petroleum Exploration & Development, PetroChina, Beijing 100083, China
[e] Qinghai Oilfield Company, PetroChina, Dunhuang 736202, China

ARTICLE INFO

Keywords:
Natural laumontite
Volcanic material alteration
Diagenetic sequence
Laumontite stability
Hydrocarbon reservoirs
Non-marine petroliferous basins in China

ABSTRACT

Laumontite is a calcium-rich zeolite that typically occurs as an authigenic mineral in sedimentary rocks. Due to its specific formation conditions and its high instability in acidic environments, laumontite provides a key geological indicator for analysing sedimentary-diagenetic system and identifying high-quality reservoirs in middle-deep strata. This study offers a comprehensive review of the distribution, occurrence, chemical composition, genesis, controlling factors, and the impacts on hydrocarbon reservoirs of laumontite in the sedimentary rocks of typical non-marine basins in China, such as the Junggar Basin, the Ordos Basin, and the Sichuan Basin. Previous research indicates that laumontite commonly develops as a continuous or patchy cement, fracture filling, and replacement product within vertically stacked deltaic subaqueous distributary channels. Sandstones enriched in plagioclase or volcanic material are considered ideal host rocks for laumontite formation. During eodiagenesis (<85 °C), laumontite extensively fills intergranular pores, with individual crystals typically exhibiting a long prismatic habit, and commonly occurring in association with clay minerals, quartz, and heulandite. During mesodiagenesis (85–175 °C), laumontite occurs as patchy intergranular fillings, with individual crystals progressively developing a short prismatic morphology, and is mainly associated with calcite, illite, quartz, and albite. Laumontite in sedimentary rocks is typically characterised by a low Si/Al ratio (2.00–2.20), and its chemical composition shows no systematic variation with temperature or occurrence. Formation mechanisms of laumontite include the albitisation of plagioclase, transformation of volcanic material, and alteration of early-formed zeolites. Incomplete transformation of plagioclase may result in a higher Si/Al ratio in laumontite. Fluid inclusion homogenisation temperature data indicates laumontite in sedimentary rocks primarily forms within a temperature range of 60–140 °C. The transformation of plagioclase and volcanic material to laumontite can proceed throughout this interval, while alteration of heulandite to laumontite generally requires temperatures above 90 °C. High pH, low pCO_2 and Ca-rich pore fluids are key factors controlling laumontite formation, while the presence of Na^+ lowers the equilibrium temperature of laumontite-forming reactions. Although early-formed laumontite occupies primary pores, it also contributes to compaction resistance. Owing to its well-developed cleavage and large internal pore volume, laumontite dissolves more readily in acidic fluids than K-feldspar, albite, or other aluminosilicates. Its dissolution zone provides a favourable environment for hydrocarbon accumulation. Additionally, the internal cavities within laumontite crystals possess a large specific surface area, which enables strong physical adsorption of methane molecules.

* Corresponding author at: National Key Laboratory of Petroleum Resources and Engineering, China University of Petroleum (Beijing), Beijing 102249, China.
E-mail address: sfzhu@cup.edu.cn (S. Zhu).

https://doi.org/10.1016/j.earscirev.2025.105197
Received 28 January 2025; Received in revised form 14 June 2025; Accepted 16 June 2025
Available online 17 June 2025

Contents

1. Introduction

Zeolite was first synthesised and named by a Swedish scientist in 1756, but natural zeolites were not discovered in volcanic rocks until the 1950s. Since then, extensive research has been conducted on the structure, composition, and genesis of various types of zeolite minerals (Hay, 1966; Hay and Sheppard, 2001; Bloch and Helmold, 1995; Stewart and Mcculloh, 1977). Zeolites are aluminosilicate minerals with a framework consisting primarily of Si—O and Al—O tetrahedron. Cavities and channels typically account for more than 50 % of the total crystal volume (Hay, 1966). Zeolites can be classified into high-silica and low-silica types based on their Si and Al content, and they commonly exhibit vertical zonation—transitioning from high-silica zeolites in shallow layers to low-silica types at greater depths (Iijima, 2001; Sun and Cao, 1991). Laumontite is a representative low Si/Al ratio zeolite. For several decades, laumontite has been regarded as an

Table 1
Characteristics of laumontite-bearing strata in typical basins worldwide.

Locality	Age	Basin and Region	Basin type	Depositional environment	Rock Types	Depth (m)	Geothermal gradient (°C/100 m)	Volume content (%)	References
America	Oligocene	San Emigdio area of San Joaquin Basin	Foreland basin	Deep-sea	Arkose/Lithic arkose	>1525	3.0–3.5	0–24/18	Bloch and Helmold (1995)
	Miocene	North Tejon oil fields of San Joaquin Basin	Foreland basin	Deep-sea	Arkose	2642–3408	/	1–25	Noh and Boles (1993)
	Paleogene	Santa Ynez basin	Foreland basin	Marine	Arkose	2515–5669	/	1–15	Helmold and Van (1984)
Japan	Eocene	Yufutsu field of south-central Hokkaido	Fore-arc basin	Fluvial	Conglomerate	4200–4800	2.9	12.5	Yanagimoto and Iijima (2006)
	Neogene	Niigata Oil Field of Northern Honshu	Back-arc basin/Rift basin	Deep-sea	Arkose	3500–4500	3.3	/	Iijima and Utada (1974)
Faeroe islands	Late Paleocene-Early Eocene	Rosebank field of Faraeo-Shetland basin	Rift basin	Fluvial-delta	Arkose/Lithic arkose	2800–3000	5.1	4–14	Sætre et al. (2018)
Argentina	Cretaceous	Southwestern flank of the Golfo de San Jorge Basin	Rift basin	Lacustrine and fluvial	Arkose/Lithic arkose	>2500	2.5–3.5	0–14.6	Limarino et al. (2017)

indicator of low-grade metamorphism (Kossovskaya and Shutov, 1965; Winkler, 1979). Its presence was long considered the 'death line' for petroleum, a phenomenon petroleum geologists sought to avoid. However, by the late 20th century, with technological advancements and increased research, more geoscientists recognised that laumontite can form at lower temperatures (Helmold and Van, 1984; Wopfner et al., 1991; Noh and Boles, 1993; Civitelli et al., 2024). Homogenisation temperatures of fluid inclusions suggest that laumontite may begin to form at temperatures below 100 °C, possibly as low as 60–70 °C (Yang and Qiu, 2002). This indicates that laumontite precipitation can occur prior to intense compaction and before the influx of organic acids and hydrocarbons (Yang and Qiu, 2002; Wang et al., 2022a). Laumontite in sedimentary rocks is commonly observed in sandstones and conglomerates rich in volcanic material or plagioclase, but is scarce in siltstones and mudstones (Iijima,1988, Koporulin, 2013, Zhu et al., 2014a). It primarily occurs as cement or replacement product during burial diagenesis (Helmold, 1979; Iijima, 2001; Wang et al., 2004). Due to its susceptibility to dissolution under acidic conditions—which enhances hydrocarbon reservoir quality (Zhu, 1985; Iijima, 2001)—laumontite is significant for mid- and ultra-deep oil and gas exploration.

International research on laumontite in sedimentary rocks have primarily examined marine and fluvial depositional environments. Table 1 summarises key characteristics of representative laumontite-bearing basins. Early studies concentrated on zeolites in volcaniclastic rocks, detailing vertical zonation patterns and the transformation sequence from volcanic glass to zeolites (Coombs, 1954; Iijima and Utada, 1974; Iijima, 1988; Ogihara, 1996). The transformation of heulandite to laumontite under alkaline conditions is recognised as a major formation pathway. Albitisation of plagioclase also provides essential material sources for laumontite precipitation (Coombs, 1954; Coffman, 1988; Noh and Boles, 1993). Although early laumontite precipitation may enhance the potential for later dissolution, analysis of clastic rocks in the Los Angeles Basin by Coffman (1987) revealed that secondary pores are well developed in calcite-cemented zones but remain limited

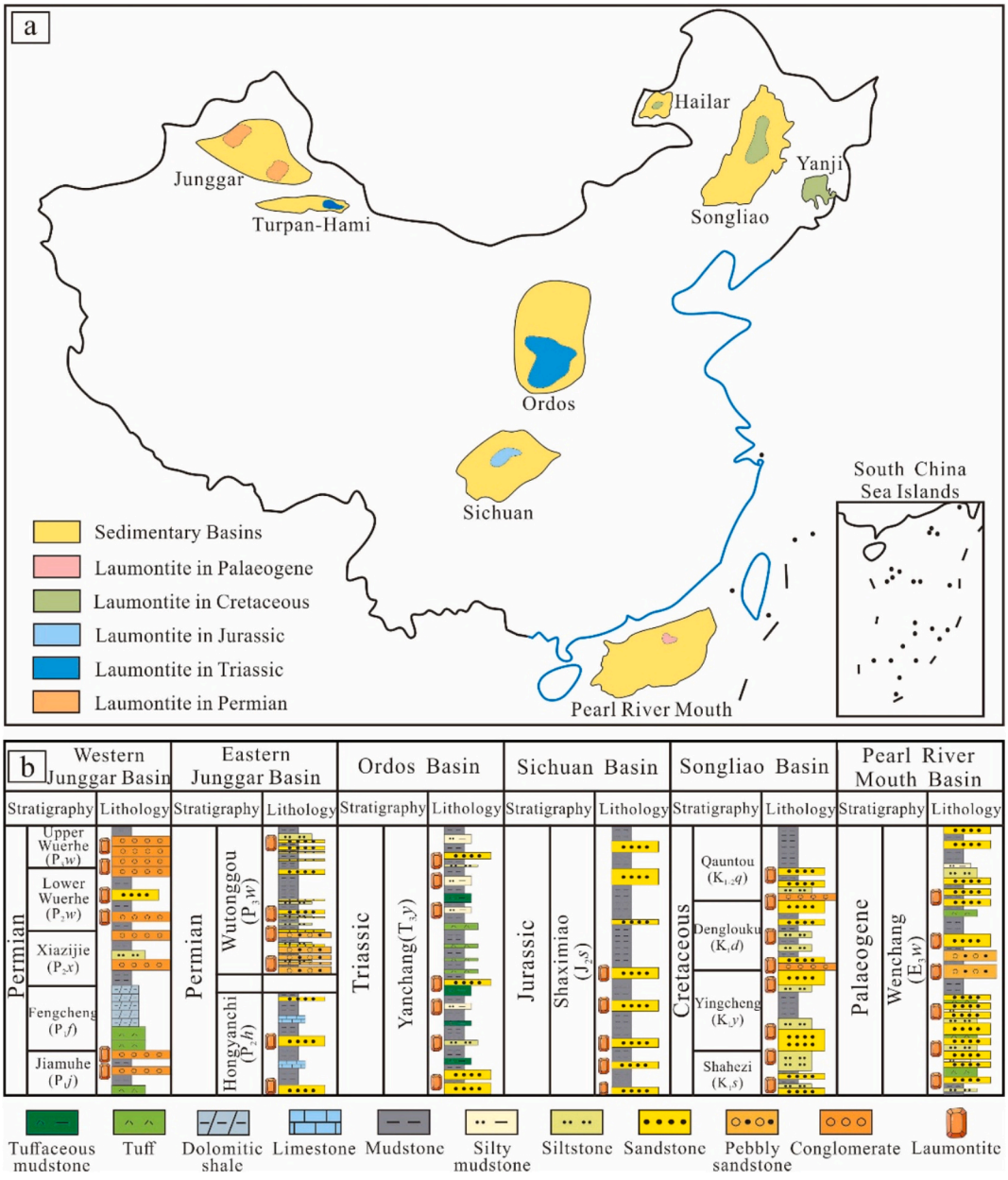

Fig. 1. Simplified map showing the non-marine petroliferous basins in China from where laumontite has been reported in sedimentary rocks (a). Histogram showing the lithological types of rocks hosting laumontite in the major basins of China (b).

Table 2
Main laumontite-bearing formations in the non-marine petroliferous basins in China.

Stratigraphy	Formation	Abbreviations	Basin and Region	Basin type	Depositional environment	Rock Types	Depth/m	Geothermal gradient (°C/100 m)	Volume content/ %	References
Palaeogene	Wenchang Fm.	E_3w	Huizhou Sag of Pearl River Mouth Basin	Rift Basin	Fan Delta	Arkose	3000–4200	3.35	$\frac{1-24}{6}$	Ma et al. (2023); Jin et al. (2023)
Cretaceous	Yingcheng Fm.	K_1y	Changling, Lishu and Dehui Fault Depression of Songliao Basin	Rift Basin	Fan Delta	Arkose	1500–4100	3.5–4.0	$\frac{1-32}{4}$	Zhang et al. (2016); Hu et al. (2018); Yang et al. (2017); Guo (2018)
	Shahezi Fm.	K_1s	Lishu Fault Depression of Songliao Basin	Rift Basin	Fan Delta	Arkose	2000–4000	3.5–4.0	$\frac{0-3}{1}$	Chen (2017); Hou (2022)
	Quantou and Denglouku Fm.	K_1q and K_1d	North Songliao Basin	Rift Basin	Fan Delta	Lithic arkose/ Feldspathic lithic sandstone	2000–4000	3.80	$\frac{1-28}{8}$	Xing and Zhang (1982); Yang et al. (1991); Yang et al. (2002); Wang et al. (2004)
	Dalazi and Tongfosi Fm.	K_1d and K_1t	Yanji Basin	Rift Basin	Fan Delta	Arkose	1400–3300	/	/	Yu et al. (2012b)
	Nantun and Tongbomiao Fm.	K_1n and K_1t	Wuerxun - Beier Sag of Hailaer Basin	Rift Basin	Fan Delta	Arkose	500–2000	3.44–4.20	$\frac{1-13}{5}$	Cui (2007); Yu et al. (2012a)
Jurassic	Shaximiao Fm.	J_2s	Central and Northeastern Sichuan Basin	Cratonic Basin	Delta	Feldspathic lithic sandstone/ Lithic arkose	1600–2200	2.27	$\frac{1-17}{3}$	Qing et al. (2020); He et al. (2023); Xiao et al. (2023); Chen et al. (2024); Tan et al. (2024)
Triassic	1th to 4th of Yanchang Fm.	T_3y^{1-4}	Ordos Basin	Cratonic Basin	Braided River Delta	Arkose/ Lithic arkose	500–3000	2.80	$\frac{1-25}{3}$	Yang et al. (2002); Bai et al. (2009); Fu et al. (2010); Zhou (2019); Yuan et al. (2020); Wang et al. (2022a); Fu et al. (2022)
	Keymay Fm.	T_2k	Hami Sag of Turpan-Hami Basin	Rift Basin	Fan Delta	Feldspathic lithic sandstone/ Lithic arkose	3800–4500	2.95–3.29	12	Liu (1996)
Permian	Wutonggou Fm.	P_3w	Fukang Sag of Junggar Basin	Foreland Basin	Fan Delta	Arkose	1500–6000	2.60	$\frac{2-15}{7}$	Wang et al. (2018); Shan et al. (2023)
	Jiamuhe Fm.	P_1j	Zhongguai Uplift and Shawan Sag of Junggar Basin	Rift Basin	Fan Delta	Arkose	3000–7000	2.12	$\frac{1-36}{9}$	Cai (2016); Li (2019); Guo et al. (2022); Zhou et al. (2023); Zhao et al. (2023)
	Weuerhe Fm.	$P_{2\text{-}3}w$	Zhongguai Uplift, Mahu and Shawan Sag of Junggar Basin	Rift-Foreland Basin	Fan Delta	Arkose	1900–7000	2.12	$\frac{2-16}{4}$	Lian and Yang (2017); Li (2019); Yan (2019); Guo et al. (2022); Sun et al. (2023); Qin et al. (2023b)
	Hongyanchi Fm.	P_2h	Chaiwopu Sag of Junggar Basin	Rift Basin	Fan Delta	Arkose	3000–4500	2.60	$\frac{0-3}{1}$	Yu et al. (2016)

Volume content: $\frac{\text{Min}-\text{Max}}{\text{avg}}$.

in laumontite-cemented zones. This contrast is likely the result of selective dissolution by diagenetic fluids. Additionally, hydrothermal laumontite in sandstones has been widely studied (Vincent and Ehlig, 1988; Hall and Moss, 1997). It typically precipitates within intergranular pores and early-formed microfractures. Subsequent tectonic activity may reopen laumontite-filled veins, increasing the potential for high-quality hydrocarbon reservoirs (Yanagimoto and Iijima, 2006). However, late-stage hydrothermal laumontite can have a detrimental impact on reservoir rocks (Remy, 1994).

Although research on laumontite in China started relatively late, its important role in hydrocarbon reservoir formation has attracted increasing attention over the past three decades, leading to significant progress in understanding its formation and distribution (Zhu, 1985; Yang et al., 1991; Zhang, 1992; Fu et al., 2010; Meng et al., 2020; Zhu et al., 2020; Fu et al., 2022; Chen et al., 2024). Currently, laumontite has been reported across a wide range of basins in China (Fig. 1), including the Permian of the Junggar Basin, the Jurassic of the Sichuan Basin, the Triassic of the Ordos Basin, and the Cretaceous of the Songliao, Yanji, and Hailaer basins, as well as the Paleogene of the Pearl River Mouth Basin. Laumontite in sedimentary rocks across various Chinese regions predominantly forms in lacustrine-deltaic environments. Detailed geological backgrounds of each basin are provided in Table 2. Laumontite occurs at buried depth of 500–7000 m, with an average volume content of about 4–6 % and a maximum recorded value of 36 %. The host rocks are primarily arkose and feldspar lithic sandstones, classified according to the scheme proposed by Folk (1968). Among these, the Yanchang Formation of the Ordos Basin and the Permian of the Junggar Basin, exhibit the most extensive laumontite development, whereas the Wenchang Formation of the Pearl River Mouth Basin shows only limited occurances. Notably, the sandstones of the Yanchang Formation in the Ordos Basin contain a relatively low proportion of volcanic material. Ongoing research has highlighted the strict formation conditions and complex distribution patterns of laumontite. Moreover, a clear correlation has been observed between laumontite content and reservoir porosity (Bai et al., 2009; Qi, 2013; Chen et al., 2024). This has prompted increased attention in the mechanisms of laumontite formation and dissolution, in order to clarify its intrinsic relationship with high-quality hydrocarbon reservoirs. These insights aim to offer more accurate guidance for oil and gas exploration.

This study provides a comprehensive review of research on laumontite in sedimentary rocks from continental lacustrine basins in China, focusing on its distribution, occurrence, chemical composition, and associated minerals. By integrating thin section petrography, scanning electron microscopy (SEM), electron probe microanalysis (EPMA), and fluid inclusion thermometry, this study investigates the genesis and evolutionary models of laumontite in sandstone and conglomerate, as well as its implications for hydrocarbon reservoir quality. The findings provide a theoretical basis for understanding diagenetic systems in volcanic-sedimentary basins and the formation mechanisms of high-quality laumontite-bearing reservoirs in middle to ultra-deep strata.

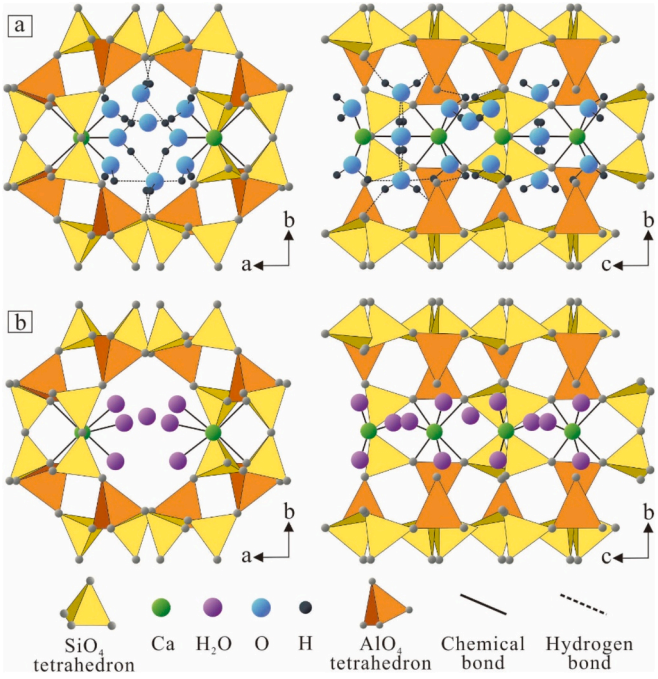

Fig. 2. Tetrahedral models of highly (a) and lowly (b) hydrated laumontite structures (modified from Rashchenko et al., 2012).

2. Laumontite mineralogy

Laumontite ($Ca_4[Al_8Si_{16}O_{48}]\cdot 16H_2O$), a calcium-rich zeolite, possesses a crystal framework composed of four- or six-membered rings formed by Si—O and Al—O tetrahedron, along with metal cations and H_2O molecules (a = 7.57 Å, b = 13.10 Å, c = 14.75 Å, β = 111.5°) (Fig. 2). Laumontite has a Mohs hardness of approximately 3–3.5 and is characterised by a brittle texture, making it prone to fracturing. Due to its lower Si/Al ratio compared to other common zeolites in sedimentary rocks—such as analcime—laumontite possesses a larger cavity volume and pore size within its crystal structure (Pan et al., 2015), which facilitates the penetration of acidic fluids. Laumontite can reversibly transition between a low-hydration state (12–14 H_2O) and a high-hydration state (16–18 H_2O) in response to fluctuations in temperature and humidity. The low-hydration form is commonly referred to as 'leonhardite' (Rashchenko et al., 2012). Although dehydration does not alter the crystal lattice, it may result in reduced transparency and a lower refractive index. Upon rehydration to its original level, the physical properties are typically restored (Yang, 2014). Similar to feldspar, the substitution of Na^+ and K^+ for Ca^{2+} in laumontite is possible. When small amounts of Na^+ and K^+ replace Ca^{2+} and enter the crystal lattice, they modify the crystal structure and influence the incorporation of H_2O molecules (Baur et al., 1997; Rashchenko et al., 2012). This type of laumontite can be referred to as 'Na, K-rich laumontite' with simplified stoichiometry $[(Ca_{2.6}Na_{1.2})K_{1.6}(H_2O)_{14}][Al_8Si_{16}O_{48}]$.

Laumontite belongs to the monoclinic crystal system. Under plane-polarised light, it appears colorless with low negative relief and exhibits two sets of nearly vertical cleavages. In cross-polarised light, it displays interference colours ranging from grayish white to pale yellow, accompanied by oblique extinction. Laumontite typically forms prismatic crystals, which may gradually transition to pseudoisometric or pseudorhombohedral habits with increasing temperature and decreasing supersaturation (Kostov, 1967) (Fig. 3a). Ghobarkar and Schäf (1998) synthesised laumontite under laboratory conditions at 30–365 °C and 1 kbar H_2O pressure. They concluded that long prismatic laumontite crystals are characteristic of low-temperature growth, whereas short prismatic crystals form at higher temperatures (Fig. 3b-d). At 250 °C, two distinct crystal morphologies were observed, suggesting the initiation of a second generation of laumontite formed through dissolution and re-precipitation. Furthermore, with increasing temperature, the crystals exhibited progressive shortening along the c-axis. In natural settings, laumontite commonly occurs in sedimentary rocks as columnar, fibrous, or radiating aggregates (Fig. 3e, f) (Goodell, 1969; Wang et al., 2022b; Zhou et al., 2023).

3. Occurrences and associated authigenic phases

Laumontite primarily forms during the late eodiagenetic and early mesodiagenetic stages, with the latter also marking the main phase of laumontite dissolution. During early eodiagenesis, laumontite first appears as continuous cement, fracture filling, and replacement product, a process that continues into stage B. Following the onset of

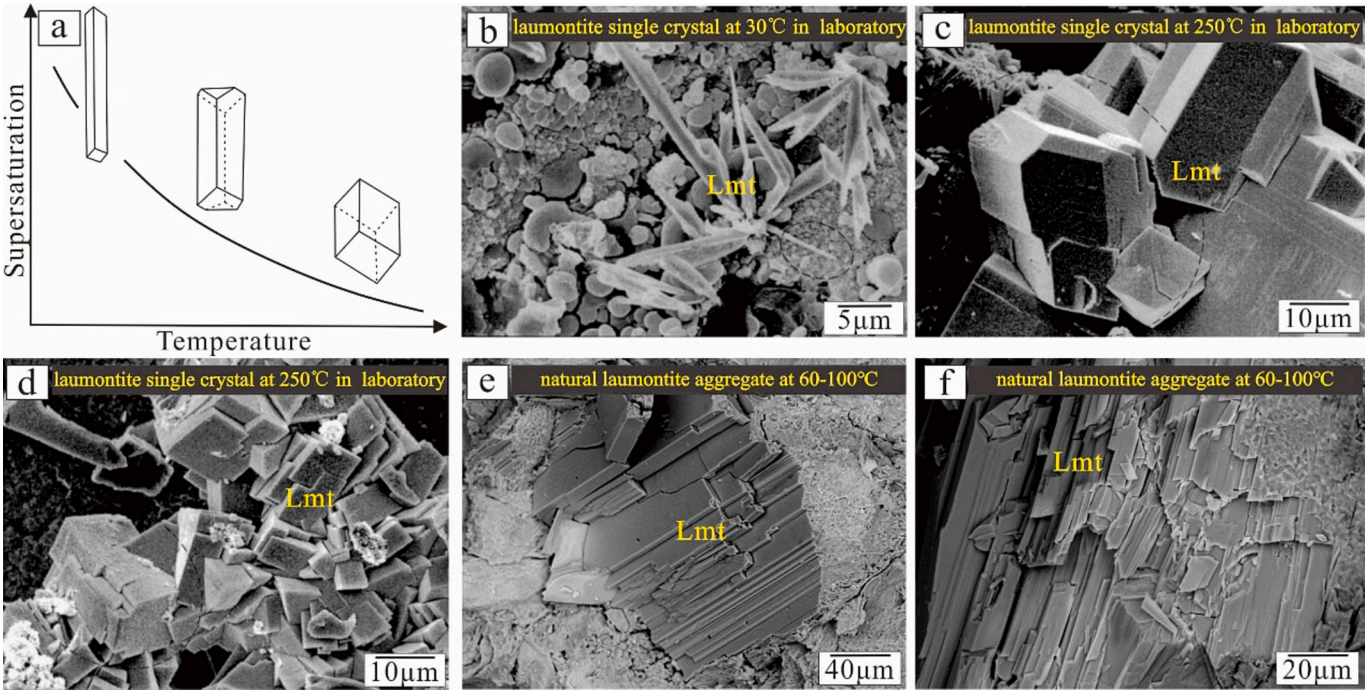

Fig. 3. Crystal habits of laumontite. (a) Crystal structures of natural laumontite at different temperatures and saturations. (b) Synthetic single crystal at 30 °C. (c, d) Synthetic single crystal at 250 °C. (e, f) Natural laumontite aggregates formed at 60–100 °C. Lmt: laumontite. a-d: from (Kostov, 1967; Ghobarkar and Schäf, 1998).

Table 3
Characteristics and Associated authigenic phases of laumontite in different diagenetic stages.

Diagenetic stages	Crystal form	Occurrence	Associated authigenic phases	Genesis	temperature
Early eodiagenesis (+)	Long prismatic	Continuous cement, fracture filling, replacement product	I/S, chlorite, quartz	albitization of plagioclase, transformation of volcanic material	<65 °C
Late eodiagenesis (+++)	Long prismatic	Continuous cement, fracture filling, replacement product	chlorite, quartz, albite	albitization of plagioclase	65–85 °C
			chlorite, quartz, heulandite	transformation of volcanic material	
Early mesodiagenesis (+++) (−-)	Long prismatic, short prismatic	patchy cement, fracture filling, replacement product	calcite, quartz, illite, albite	albitization of plagioclase	85–140 °C
			heulandite, calcite, quartz, illite, albite	transformation of volcanic material	
			heulandite, calcite, quartz, illite	transformation of early zeolite	
Late mesodiagenesis (+) (−)	short prismatic	fracture filling, replacement product	calcite, quartz, kaolinite, illite	transformation of early zeolite	140–175 °C

(+) The formation of laumontite, (−) the dissolution of laumontite.

mesodiagenesis, continuous compaction and early cementation result in a significant loss of primary porosity. Consequently, laumontite predominantly occurs in the form of patchy cement, fracture filling, or as a replacement product. Over the full diagenetic history, laumontite is closely associated with minerals such as chlorite, illite, montmorillonite, quartz, heulandite, calcite, and albite. The assemblage of laumontite-associated minerals varies across different diagenesis stages (Table 3).

3.1. Continuous and patchy cement

During early diagenesis, continuous laumontite cement forms extensively, consistently filling primary pores (Fig. 4a-c) and displaying well-developed cleavage (Fig. 4d-f). This type of laumontite is mainly found in sandstones with high laumontite content, where clastic grains are predominantly in point contact. It has been observed in the Shaximiao Formation of the Sichuan Basin and the Yanchang Formation of the Ordos Basin, at present-day burial depths ranging from approximately 500 to 4000 m.

Patchy laumontite forms during the middle to late stages of diagenesis and is characterised by irregular, scattered, and uneven distributions among detrital particles, typically exhibiting indistinct cleavage (Fig. 4g). The size and morphology of the crystals are influenced by the surrounding pore structure (Fig. 4h), with clastic grains generally displaying point or linear contacts. This type of laumontite is commonly observed in the Wenchang Formation of the Pearl River Mouth Basin, the Cretaceous of the Songliao and Hailar Basins, and the Permian of the Junggar Basin, at burial depths ranging from approximately 2000 to 7000 m.

The formation of laumontite cement is controlled not only by diagenetic stage and burial depth, but also by the structural maturity and initial porosity of the host rock. High-maturity sandstones typically favour the development of continuous cement, while low-maturity sandstones with limited initial porosity tend to develop patchy laumontite.

3.2. Fracture filling

Fracture-filled laumontite is relatively common in volcanic rocks and

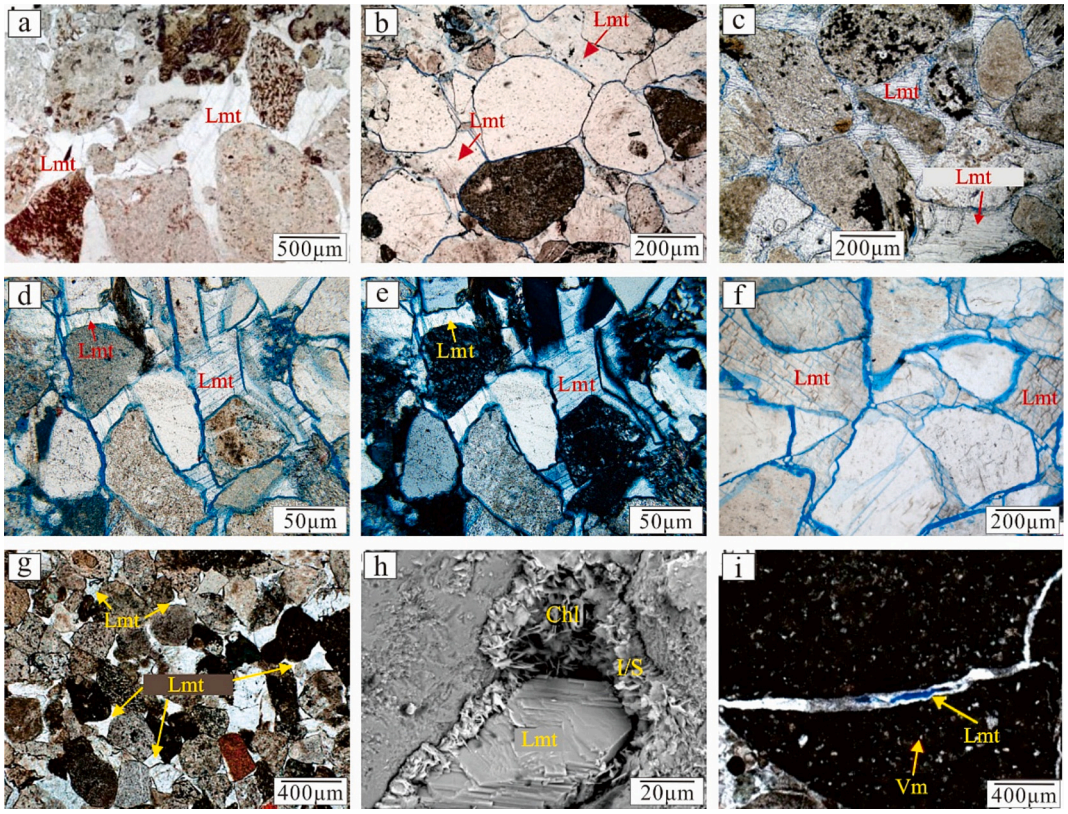

Fig. 4. Occurrences of laumontite in sedimentary rocks from continental lacustrine basins in China: (a-f) continuous cement, (g-h) patchy cement and (i) fracture-filled laumontite. (a) Well ZJ6, 4879.5 m, P_1j in Shawan sag of Junggar Basin. (b) Well ZQ1, 2654.5 m, J_2s in central region of Sichuan Basin. (c) Well B201–1, 3222.96 m, K_1y in Longfengshan region of Songliao Basin. (d-e) Well W155, 2379.5 m, T_3y^2 in Longdong region of Ordos Basin. (f) Well JQ16, 2742.12 m, J_2s in central region of Sichuan Basin. (g) Well F48, 4511 m, P_3w in Zhundong region of Junggar Basin. (h) Well X462, 2223.8 m, T_3y^1 in Shanbei region of Ordos Basin. (i) Well M218, 3948.23 m, P_2w in Mahu region of Junggar Basin. Lmt: laumontite; Chl: chlorite; I/S: mixed layer; Vm: volcanic material. a-c: from (Liu et al., 2017; Wang et al., 2022b; Zhou et al., 2023). f-i: from (Chen et al., 2019b; Yan, 2019; Qin et al., 2023a; Chen et al., 2024).

often associated with hydrothermal activity (Hall and Moss, 1997; Liang et al., 2011; Nan et al., 2016). However, its distribution is limited in lacustrine sedimentary rocks of continental basins in China, with reported cases confined to volcanic-rich sandstones of the Wuerhe Formation in the Mahu Depression, Junggar Basin (Fig. 4i). Fracture-filled laumontite has been observed to form contemporaneously with intergranular laumontite (Yan, 2019). In the Santa Ynez Mountains of California, fracture-filled laumontite is also developed in feldspar-rich sandstones. These fractures can reach widths of up to 2 mm and extend several tens of centimetres in length. They are interpreted to have formed during late diagenesis, which closely corresponds to the main period of laumontite precipitation (Helmold, 1979).

3.3. Replacement of grains or volcanic matrix

The replacement of other materials by laumontite is also a common diagenetic feature, involving plagioclase, volcanic material, quartz grains, and early-formed zeolites. The replacement of plagioclase by laumontite typically initiates along twinning planes and cleavage fractures or progresses inward from grain edges (Fig. 5a-c) (Li et al., 2005; Chen et al., 2019a, 2019b). In regions of extensive replacement, laumontite may encapsulate inclusions of sericite or epidote, which are typically formed through the alteration of plagioclase. In volcaniclastic sequences, laumontite preferentially replaces two main components: volcanic glass within volcanic fragments and volcanic ash between larger particles (Fig. 5d, e). In contrast to the frequent replacement of plagioclase and volcanic material, the replacement of quartz grains is exceptionally rare, occurring only locally in the Shaximiao Formation of the Sichuan Basin (Fig. 5f). Additionally, the replacement of early-formed zeolites, such as heulandite, represents another significant type. This replacement process can take place concurrently with intergranular cementation, as they share similar formation conditions.

3.4. Associated authigenic phases of laumontite

Clay minerals, including illite-smectite mixed-layer (I/S), illite, kaolinite, and chlorite, are the principle minerals associated with laumontite. Their formation is facilitated by the hydration of volcanic material, the alteration of biotite, and ion migration from adjacent mudstones. During early diagenesis, I/S and illite commonly develop along grain margins, forming rim-like coatings. Then chlorite and laumontite fill the pores enclosed by these coatings (Fig. 4h). In the late stage, illite and kaolinite may develop as secondary minerals resulting from laumontite dissolution. Chlorite commonly occurs as a pore-lining or pore-filling phase in laumontite-bearing sandstones (Fig. 6a, b), with pore-lining chlorite being more widespread and typically forming before quartz overgrowths and zeolite minerals. In contrast, pores-filling or replacement chlorite forms later but exhibits better crystallinity. Electron microprobe analyses show that chlorite associated with laumontite is iron-rich (24–28 wt%) and magnesium-poor (8–9 wt%) (Bai et al., 2009; Qing, 2020; Hong et al., 2022). Among these, chlorite from the Yanchang Formation in the Ordos Basin has the lowest iron content (24 wt%), reflecting the limited input of volcanic material and the insufficient supply of Fe and Mg ions in the region.

The hydrolysis of volcanic material releases a large amount of dissolved SiO_2(aq), and the alteration of plagioclase also contributes to its generation. During early diagenesis, some of the SiO_2(aq) precipitates as quartz overgrowths (Fig. 6c), typically forming earlier than laumontite

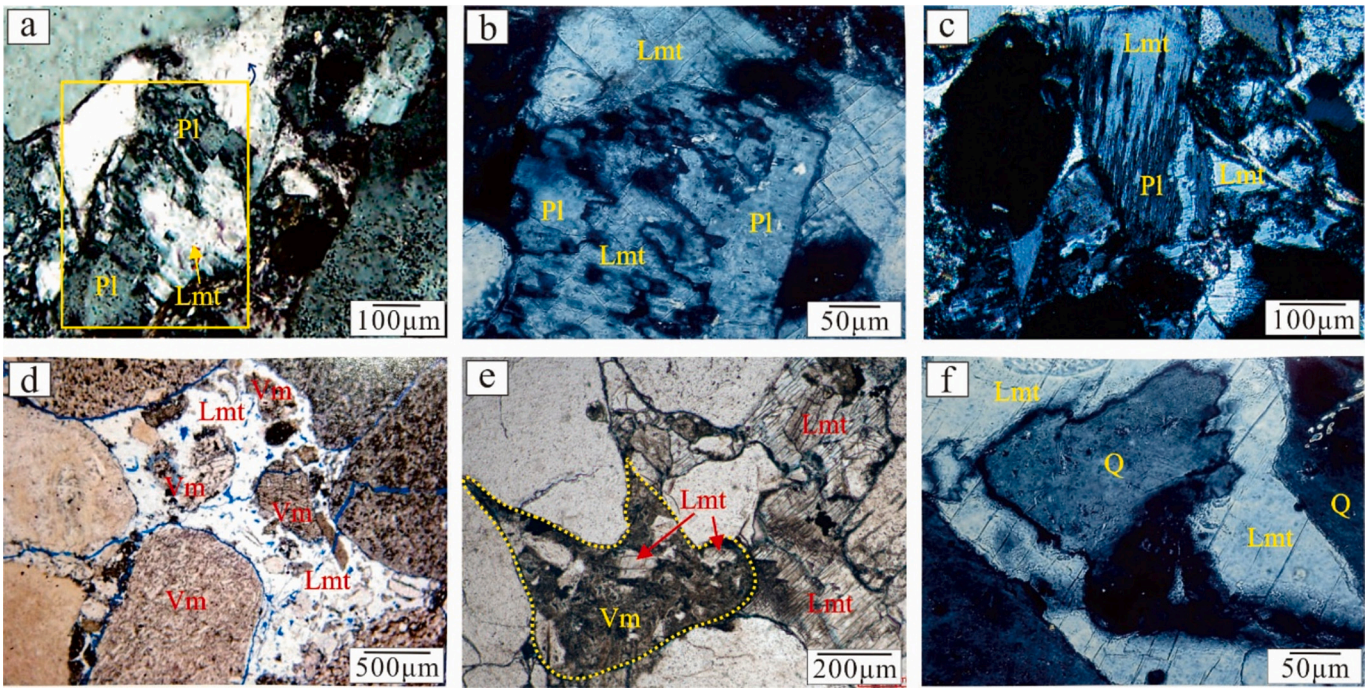

Fig. 5. Laumontite replaceing plagioclase(a-c), volcanic material(d-e) and quartz(f) in sedimentary rocks of continental lacustrine basins in China. (a) Well Q5, 1083.3 m, T_3y^3 in Ordos Basin. (b) Well SH1, 2190.1 m, J_2s in central region of Sichuan Basin. (c) Well B420, 2426.9 m, T_3y^2 in Longdong region of Ordos Basin. (d) Well K80, 4155.69 m , P_2w in northwest region of Junggar Basin. (e) Well YQ1, 2162.9 m, J_2s in central region of Sichuan Basin. (f) Well SH1, 2190.1 m, J_2s in central region of Sichuan Basin. Pl: plagioclase; Lmt: laumontite; Vm: volcanic material; Q: quartz. a: from (Wang et al., 2022a). e: from (Chen et al., 2024).

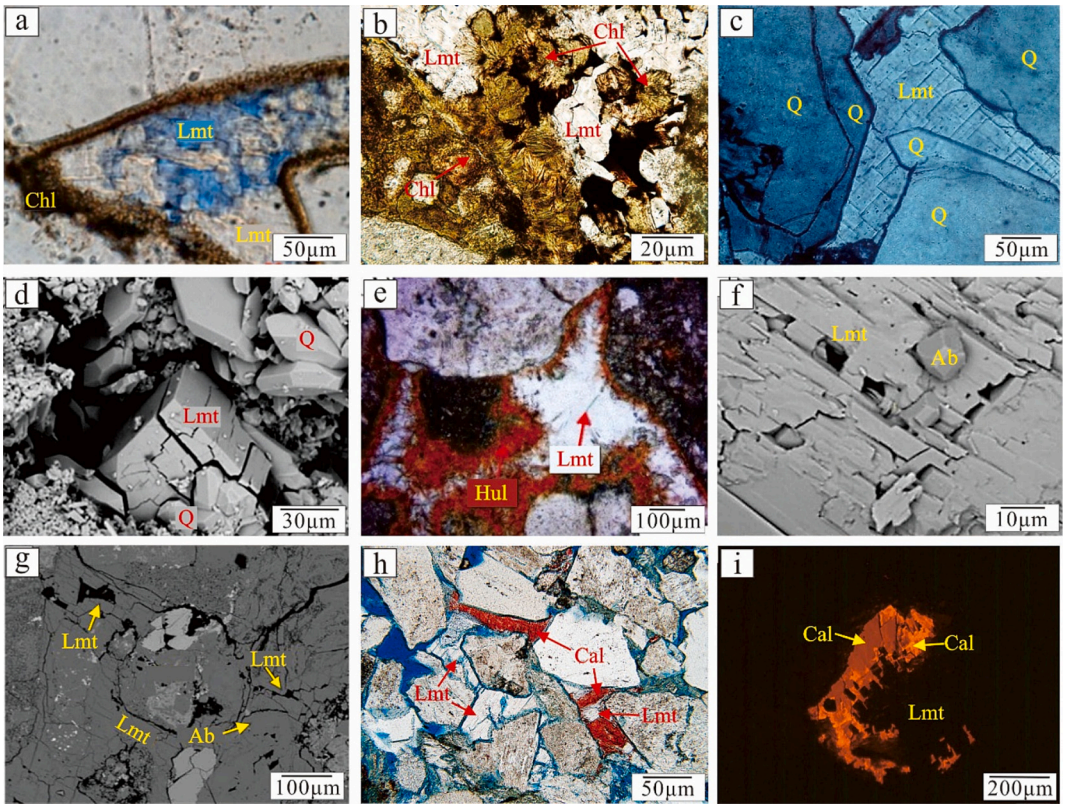

Fig. 6. Characteristics of chlorite(a-b), quartz(c-d), heulandite(e), albite(f-g) and calcite(h-i) associated with laumontite in sedimentary rocks of continental lacustrine basins in China. (a) Well H411, 1261.17 m, T_3y^3 in southeastern Ordos Basin. (b) Well XX, P in Junggar Basin. (c) Well SH1, 2190.1 m, J_2s in central region of Sichuan Basin. (d) Well G3, 4760.8 m , P_3w in Mahu region of Junggar Basin. (e) Well M217, 4058.8 m, P_2w in Mahu region of Junggar Basin. (f) Well L8, 4179.8 m, K_1y in Lishu fault depression of Songliao Basin. (g) Well ZJ1, 4862.7 m, P_1j in Shawan region of Junggar Basin. (h) Well L87, 1866.9 m, T_3y^1 in Longdong region Ordos Basin. (i) Well G191, 4335 m, P_3w in Shawan region of Junggar Basin. Lmt: laumontite; Chl: chlorite; Q: quartz; Hul: heulandite; Ab: albite; Cal: calcite. a: from (Fu et al., 2022). d-g: from (Zhi et al., 2022; Yan, 2019; Hou, 2022; Zhou et al., 2023). i: from (Zhi et al., 2022).

(Fig. 6d) but later than pore-lining chlorite. Due to the increased solubility of SiO_2 under alkaline conditions, most dissolved silica is subsequently incorporated into laumontite during late diagenesis. Under acidic conditions, quartz can also precipitate in pores as a dissolution product of laumontite.

The formation of heulandite is closely associated with the alteration of volcanic material, often derived from the transformation of clinoptilolite produced by the hydrolysis of volcanic material during late eodiagenesis. It generally precedes laumontite formation and typically occurs as a pore-filling or grain-rimming phase (Fig. 6e). Heulandite primarily forms in shallow burial environments and often exhibits a reddish-brown colour due to minor Fe content. It is characterised by a high Si/Al ratio, well-developed intercrystalline pores, and a progressive decrease in abundance with increasing burial depth. At later stages, heulandite can transform into laumontite.

Authigenic albite primarily forms from the transformation of plagioclase and typically forms slightly earlier than intergranular laumontite. It commonly occurs as a replacement product or as intergranular cement (Fig. 6f, g), with pore-filling albite showing well-developed crystal forms. In sandstones and conglomerates with low plagioclase content, albite may also form through the transformation of analcime derived from volcanic material alteration, predominantly appearing as a replacement product and forming later than laumontite.

Calcite and laumontite compete for Ca^{2+} in pore fluids, and their concentrations exhibit a negative correlation (Bai et al., 2009). When laumontite content exceeds 5 % by volume, calcite content typically falls below 5 % by volume (Qing et al., 2020; Fu et al., 2022; He et al., 2023; Tan et al., 2024). Thus, calcite typically forms following the dissolution of laumontite, through the reaction of Ca^{2+}—released from laumontite—with CO_2(aq) produced during organic matter maturation. It is commonly found as intergranular cement filling dissolution pores or replacing other mineral grains (Fig. 6h, i). This type of calcite often contains elevated concentrations of FeO and MnO (Hong et al., 2022; Zhi et al., 2022). Carbon isotope data indicate a genetic link between calcite and the decarboxylation of organic matter (Fu et al., 2022; Zhou et al., 2023; Zhang et al., 2024).

Authigenic chlorite, quartz, and albite are widely distributed and may coexist with laumontite in a variety of geological settings. However, heulandite is more restricted in occurrence and absent where volcanic material is lacking. It is restricted to areas with exceptionally high volcanic input, such as the Permian of the Junggar Basin. Although calcite is widely distributed, no calcite has been observed within laumontite dissolution pores in the Wenchang Formation of the Pearl River Mouth Basin. This may be attributed to a relatively open diagenetic environment, where Ca^{2+} released from laumontite dissolution was promptly transported away by formation fluids. As a result, Ca^{2+} and CO_3^{2-} in the pore fluid may not have reached saturation conditions necessary for calcite precipitation.

4. Chemical composition of laumontite

Laumontite typically contains 49–51 wt% SiO_2, 21–22 wt% Al_2O_3, and approximately 10–12 wt% CaO (Sun and Cao, 1991). In this study, a total of 234 EPMA measurements of laumontite from sedimentary rocks across various regions of China were statistically examined. The average chemical composition of laumontite was found to be as follows: SiO_2: 52.01–53.59 wt%; Al_2O_3: 19.97–22.02 wt%; CaO: 8.67–11.41 wt%; Na_2O: 0.11–2.86 wt%; K_2O: 0.10–0.73 wt%; FeO: 0.04–0.34 wt%; and MgO: 0.01–0.38 wt%. There is no significant variation in the chemical composition of laumontite across different occurrences and regions (Fig. 7), and it generally resembles that of standard laumontite. An exception is observed in the lower Yanchang Formation in the southwestern Ordos Basin, where the average Na_2O content is higher (2.36 wt %) and the average CaO content is lower (8.67 wt%). This is attributed to the high concentrations of Na in the formation water.

The average Si/Al ratio of laumontite typically ranges from 2.01 to 2.20 and shows no significant correlation with its occurrence. A higher ratio (2.35) is observed only in the upper Yanchang Formation in the northeastern Ordos Basin. To explore this relationship, we conducted a statistical analysis of plagioclase and volcanic material contents, as well as volcanic material types, in laumontite-bearing sandstones from various regions (Table 4). The results show that the upper Yanchang Formation in the northeastern Ordos Basin contains a high proportion of plagioclase (20–40 %) but a very low content of volcanic material (<4 %). Additionally, the Si/Al ratio of laumontite tends to increase with decreasing burial depth (Zhou et al., 2023). This may be attributed to the incomplete transformation of plagioclase in shallow layers, resulting in elevated Si content and relatively lower Al content in the newly formed laumontite.

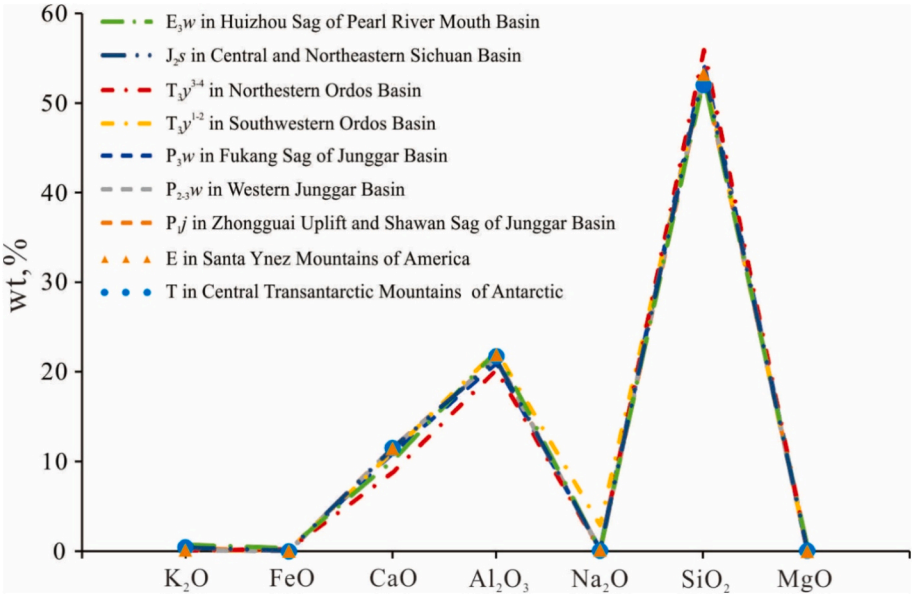

Fig. 7. Major element content of laumontite. The data are from (Helmold and Van, 1984; Vavra, 1989; Bai et al., 2009; Zhou, 2019; Fu et al., 2010; Wang et al., 2018; Hong et al., 2022; Yan, 2019; Zhi et al., 2022; Zhou et al., 2023; Li, 2019; He et al., 2023; Qing et al., 2020; Jin et al., 2023; Ma et al., 2023).

Table 4
Si/Al ratio of laumontite in lacustrine basins in China and other typical basins in the world.

Locality	Stratigraphy	Rock Types	Content/ %	Plagioclase/ %	Volcanic material/ %	SiO_2, wt%	Al_2O_3, wt%	Si/Al	Number of samples
Huizhou Sag of Pearl River Mouth Basin, China	E_3w	Arkose	$\frac{1-24}{6}$	<10	50(Tuff, Granite fragment)	$\frac{47.35-54.26}{52.01}$	$\frac{20.75-23.45}{22.02}$	$\frac{1.91-2.13}{2.01}$	14
North Songliao Basin, China	K_1q and K_1d	Lithic arkose/ Feldspathic litharenite	$\frac{1-28}{8}$	25–40	20–30 (Intermediate-acidic volcanic fragment)	52.76*	20.71*	2.20*	/
Central and Northeastern Region of Sichuan Basin, China	J_2s	Feldspathic litharenite/ Lithic arkose	$\frac{1-17}{3}$	20–35	12–30 (Intermediate-acidic volcanic fragment)	$\frac{49.72-56.39}{52.96}$	$\frac{20.35-22.27}{21.06}$	$\frac{2.05-2.24}{2.14}$	18
Southwestern Region of Ordos Basin, China	T_3y^{1-2}	Arkose/Lithic arkose	$\frac{2-20}{3}$	20–40	7–13(Volcanic fragment)	$\frac{51.66-53.83}{52.54}$	$\frac{21.58-23.00}{22.05}$	$\frac{1.96-2.10}{2.03}$	14
Northestern Region of Ordos Basin, China	T_3y^{3-4}	Arkose/Lithic arkose	$\frac{3-28}{4}$	20–40	<4(Volcanic fragment)	$\frac{48.98-58.98}{55.11}$	$\frac{16.98-22.45}{19.97}$	$\frac{2.08-2.93}{2.35}$	13
Fukang Sag of Junggar Basin, China	P_3w	Arkose	$\frac{2-15}{7}$	<10	>80(Tuff clast, andesite fragment, tuff)	$\frac{48.99-54.99}{53.59}$	$\frac{19.41-22.82}{20.69}$	$\frac{2.16-2.26}{2.20}$	24
Zhongguai Uplift and Shawan Sag of Junggar Basin, China	P_1j	Arkose	$\frac{3-36}{9}$	<10	>80(Andesite fragment, tuff clast, tuff)	$\frac{48.94-54}{52.17}$	$\frac{18.99-22.36}{21.22}$	$\frac{1.92-2.23}{2.09}$	48
Western Region of Junggar Basin, China	$P_{2\text{-}3}w$	Arkose	$\frac{2-16}{4}$	<5	>80(Tuff clast, andesite fragment, tuff)	$\frac{52.25-55.08}{52.52}$	$\frac{20.12-21.42}{21.18}$	$\frac{1.94-2.29}{2.11}$	102
Santa Ynez Mountains, America	E	Arkose	1–15	20–40	<9(Volcanic fragment)	$\frac{51.29-53.57}{52.43}$	$\frac{21.47-22.07}{21.62}$	$\frac{1.98-2.12}{2.06}$	7
Central Transantarctic mountains, Antarctica	T	Arkose	<10	20–30	20–30(Rhyolite and andesite fragment)	$\frac{50.62-52.03}{51.25}$	$\frac{21.25-21.67}{21.44}$	$\frac{1.99-2.08}{2.03}$	20

The references are the same as those given in Table 1. *The data from Yang et al., 1991. Main element content and Si/Al: $\frac{Min-Max}{avg}$.

5. Laumontite genesis

Previous studies on laumontite formation have explored a range of genetic mechanisms, including: (1) albitisation of plagioclase; (2) replacement of early-formed zeolites; (3) transformation of volcanic material; (4) reaction between calcite and kaolinite; and (5) hydrothermal alteration (Noh and Boles, 1993; Iijima, 2001). However, in the sedimentary rocks of China, laumontite formation predominantly occurs through the first three mechanisms, all of which involve zeolite generation under progressively increasing temperature conditions.

5.1. Albitisation of plagioclase

5.1.1. Formation mechanism

Laumontite can be considered a product of plagioclase albitisation, due to its similar elemental composition and structural framework. Under alkaline pore water conditions, the smaller ionic radius of Na^+ allows it to replace Ca^{2+} in plagioclase, gradually leading to albite formation. The released Ca^{2+} provides the necessary basis for laumontite precipitation. The reaction can be simplified as:

$$2CaAl_2Si_2O_8 + 2Na^+ + 4H_2O + 6SiO_2 = CaAl_2Si_4O_{12}\cdot 4H_2O + 2NaAlSi_3O_8 + Ca^{2+} \quad (1)$$

In this case, plagioclase is idealised as pure anorthite for calculation purposes, although in most sedimentary environments, plagioclase contains a certain amount of Na. Some researchers suggest that the presence of exogenous Na^+ in pore fluids is not a necessary condition for albitisation. This reaction can be represented by the following equation: (Huang et al., 2016)

$$x(NaAlSi_3O_8)\cdot y(CaAl_2Si_2O_8) + 2ySiO_2 + 4yH_2O = yCaAl_2Si_4O_{12}\cdot 4H_2O + xNaAlSi_3O_8\ (x+y=1) \quad (2)$$

Albitisation of plagioclase is often accompanied by the partial dissolution of plagioclase clasts, which provides a timely supply of SiO_2 and Na^+ for the reaction (Yang et al., 2003). This process also helps explain the genetic relationship among kaolinite, albite, and laumontite (Kaiser, 1984; Huang et al., 2001). Albitisation can occur during various diagenetic stages and provides a material basis for laumontite formation (Lander and Bonnell, 2010). A typical feature is the replacement of plagioclase by laumontite (Fig. 8a), with both laumontite and albite, as replacement products, inheriting the chemical composition of the original plagioclase (Fig. 8b, c) (Chen et al., 2024).

5.1.2. Comparison with other basins worldwide

Albitisation of plagioclase can occur across a variety of lithologies, including volcanic rocks, volcaniclastic rocks, sandstones and conglomerates. In contrast, laumontite found in the Triassic strata of the Ordos Basin (China), the Paleogene of the Santa Ynez Mountains (USA) and the Rosebank Field (Europe), and the Neogene formations of the San Joaquin Valley (USA), represents a classic non-volcanogenic type formed exclusively through plagioclase albitisation (Kaley and Hanson, 1955; Helmold and Van, 1984; Sætre et al., 2018). These representative regions share two key characteristics: (1) low volcanic material content in the host rocks, and (2) well-sorted, well-rounded detrital grains. These features result in high initial porosity, providing favourable space for both plagioclase alteration and subsequent laumontite precipitation. The formation of laumontite can span multiple diagenetic stages. Notably, Helmold and Van (1984) demonstrated, through their study of laumontite in Paleogene turbidites of the Santa Ynez Mountains, that the migration of Na^+—released during clay mineral transformation in

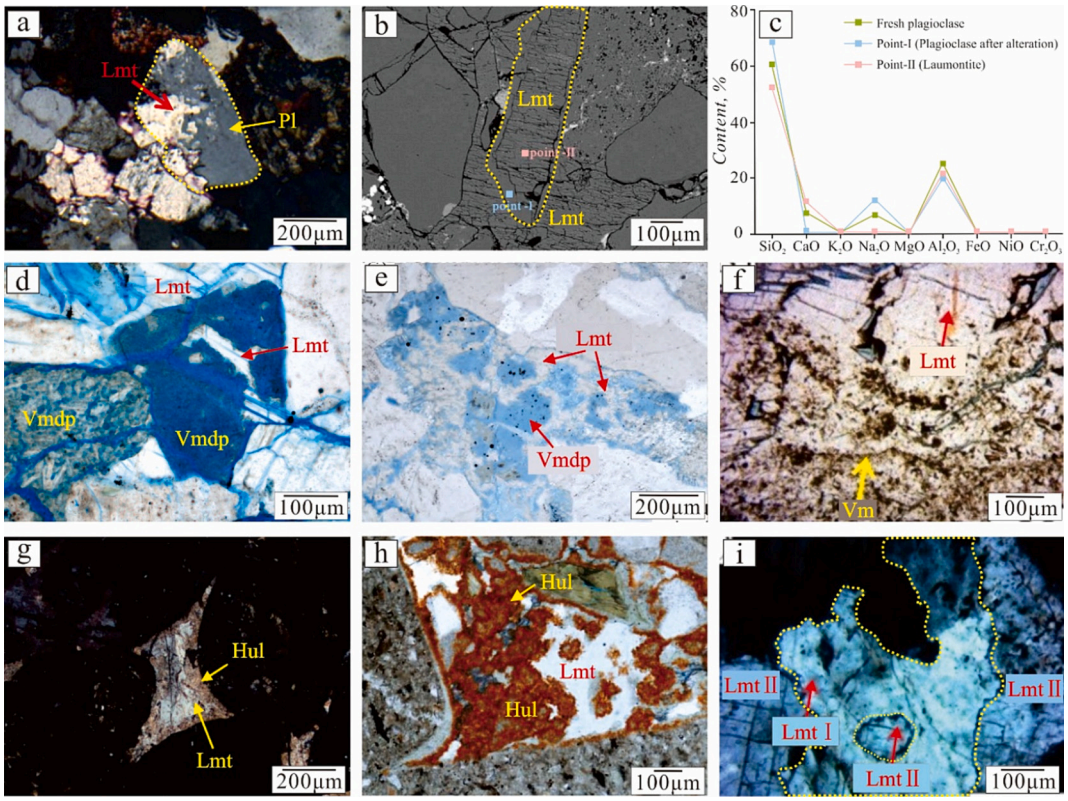

Fig. 8. Formation pathways of laumontite in sedimentary rocks from continental lacustrine basins in China: (a-c) derived from albitization of plagioclase, (d-f) directly transformed from volcanic material, and (g-i) formed through alteration of early zeolites. (a) Well D11, about 1600–2400 m, T_3y^1 in Shanbei region Ordos Basin. (b-c) The newly formed laumontite and albite have an inherited relationship with the chemical composition of the original plagioclase. Well JQ8, 2693.41 m, J_2s in central region of Sichuan Basin. (d) Well JQ16, 2746.59 m, J_2s in central region of Sichuan Basin. (e) Well HZ-26-B, 3791 m, E_3w in Huizhou sag of Pearl River Mouth Basin. (f) Well M607, 40,103.5 m, P_2w in Mahu region of Junggar Basin. (g) Well MZ7, 4463.7 m, P_2w in Mahu region of Junggar Basin. (h) Well M217, 4009.4 m, P_2w in Mahu region of Junggar Basin. (i) Well YB4, 3915 m, P_2w in Mahu region of Junggar Basin. Pl: plagioclase; Lmt: laumontite; Vm: volcanic material; Hul: heulandite; Vmdp: volcanic material dissolution pore; Lmt I: first phase of laumontite; Lmt II: second phase of laumontite. a-i: from (Zhou et al., 2023; Chen et al., 2024; Jin et al., 2023; Yan, 2019; Li et al., 2022).

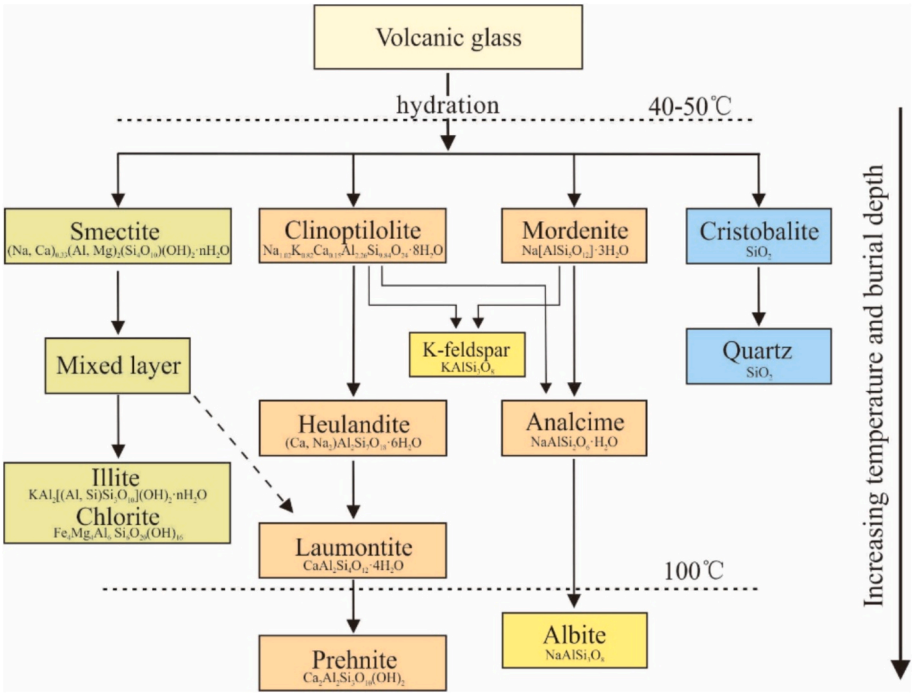

Fig. 9. Transformation sequence of volcanic material (modified from Fisher and Schmincke, 1984; Iijima, 1988; Weibel et al., 2019; Zhu et al., 2020).

mudstones—into adjacent sandstones plays a key role in accelerating plagioclase albitisation. Iijima (2001) also suggested that additional sources of Ca and Na are required for laumontite formation during plagioclase albitisation, based discrepancies between laumontite content and the chemical composition of plagioclase in the Los Angeles Basin.

5.2. Volcanic material transformation

Intergranular volcanic ash and volcanic fragments contain abundant volcanic glass, which is structurally disordered and composed of loosely connected SiO_4 tetrahedra with large intermolecular cavities. During hydration and alteration, elements can easily migrate into the pore water and participate in the formation of new minerals (Zhu et al., 2019). This process is recognised as one of the fastest low-temperature diagenetic reactions (Fisher and Schmincke, 1984). Zeolites and clay minerals are the most common alteration products of volcanic glass (Hong et al., 2017). With the continuous hydration of volcanic glass, the pH of the pore fluid gradually increases, accompanied by the enrichment of alkali metal ions and activated SiO_2 (Zhu et al., 2012). Under these conditions, laumontite can directly replace volcanic glass or precipitate from intergranular pore fluids (Fig. 8d-f). The dissolution rate of volcanic glass increases with rising salinity and alkalinity (Hay, 1966).

Previous studies have suggested that acidic volcanic fragments are generally less favourable for the formation of laumontite (Guo et al., 2022). However, this study found—through statistical analysis—that significant amounts of laumontite also developed in sandstones dominated by intermediate to acidic volcanic fragments, such as in the Shaximiao Formation of the Sichuan Basin, the Permian of the Junggar Basin, and the Cretaceous of the Songliao Basin (Table 4). In the Triassic strata of the Central Transantarctic Mountains (Antarctica), volcanic materials associated with laumontite are primarily composed of rhyolitic and andesitic clasts. In Japan, researchers conducted a statistical analysis on the relationship between volcanic rock types and laumontite occurrence, and found that laumontite can form in basic, intermediate, and acidic volcanic rocks (Iijima, 1988). Globally, laumontite formed through direct conversion of volcanic material exhibited consistent formation conditions and characteristics.

5.3. Early zeolite transformation

As previously mentioned, the alteration of volcanic material can directly provide the source for laumontite formation. Alternatively, laumontite can also form through the transformation of early-formed heulandite and related minerals. This transformation occurs under alkaline conditions rich in Ca^{2+}, and can be represented by the following reaction:

$$CaAl_2Si_7O_{18}\cdot 6H_2O = CaAl_2Si_4O_{12}\cdot 4H_2O + 3SiO_2 + 2H_2O \quad (3)$$

This process primarily takes place during early mesodiagenesis.

5.3.1. Eodiagenesis

Under low-temperature conditions, volcanic glass initially alters to montmorillonite, cristobalite, and high-hydration zeolites such as clinoptilolite and mordenite. With increasing temperature, pH, and salinity, cristobalite transforms into quartz, while montmorillonite transitions into mixed-layer clay minerals and progressively evolves toward chlorite and illite. Simultaneously, montmorillonite and cristobalite gradually convert to analcime and heulandite, accompanied by the precipitation of K-feldspar (Fig. 9).

5.3.2. Mesodiagenesis

With the initiation of mesodiagenesis, heulandite gradually transforms into laumontite, accompanied by a decreasing Si/Al ratio (Iijima, 2001). Under sustained alkaline conditions, laumontite ultimately alters to prehnite, while analcime is replaced by albite (Fig. 9). The transformation of clay minerals can provide a material basis for laumontite formation (Fisher and Schmincke, 1984). During this stage, early-formed laumontite may undergo dissolution followed by reprecipitation in response to changes in fluid composition. Microscopically, the replacement of heulandite by laumontite is a common phenomenon (Fig. 8g, h), along with localised occurrences of two generations of laumontite jointly filling the pores (Fig. 8i).

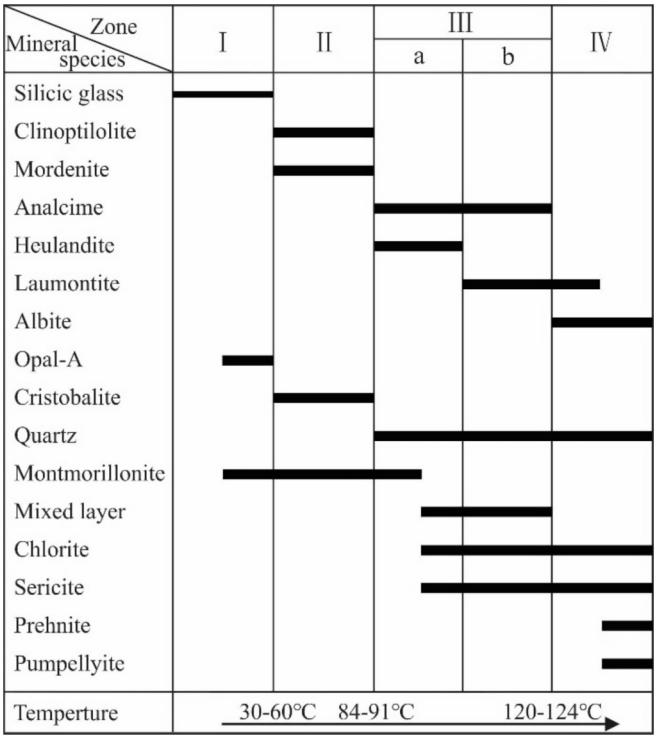

Fig. 10. Schematic diagram showing vertical zonation of zeolites and related authigenic minerals (modified from Iijima, 2001).

5.3.3. Comparison with other basins worldwide

Laumontite generated by the transformation of early-formed zeolites is also widely distributed in volcanically enriched regions. These include the Junggar Basin (China), the islands of Hokkaido, Kyushu, and Honshu (Japan), southern California (USA), the Hejre Field (Denmark), the Pechora Coal Basin, and the southwestern Transbaikal region (Russia) (Utada, 1965; Hay and Sheppard, 2001; Iijima, 2001; Koporulin, 2013; Li, 2019; Weibel et al., 2019). The transformation from heulandite to laumontite exhibits similar characteristics across these regions. Zeolite mineral assemblages resulting from the alteration of volcanic material display vertical zonation—a phenomenon extensively investigated by researchers during the last century (Yoshimura, 1961; Utada, 1965; Nakajima and Tanaka, 1967). Iijima (2001) systematically proposed four diagenetic zones: Zone I (fresh glass without zeolite), Zone II (clinoptilolite and mordenite), Zone III (analcime), and Zone IV (albite) (Fig. 10). Although the depth ranges of zeolite development often overlap, the vertical assemblages of zeolite minerals vary regionally. For example, in the Niigata oil field of Japan, analcime is absent from the zeolite assemblage (Iijima, 2001). Both the North Tejon oil field (California, USA) and Junggar Basin (China) lack clinoptilolite and mordenite (Noh and Boles, 1993; Li, 2019). These differences are likely related to variations in volcanic protolith composition and the distinct evolutionary stages of zeolite mineralisation.

5.4. Other genetic pathways

In the 20th century, some researchers proposed that calcite and

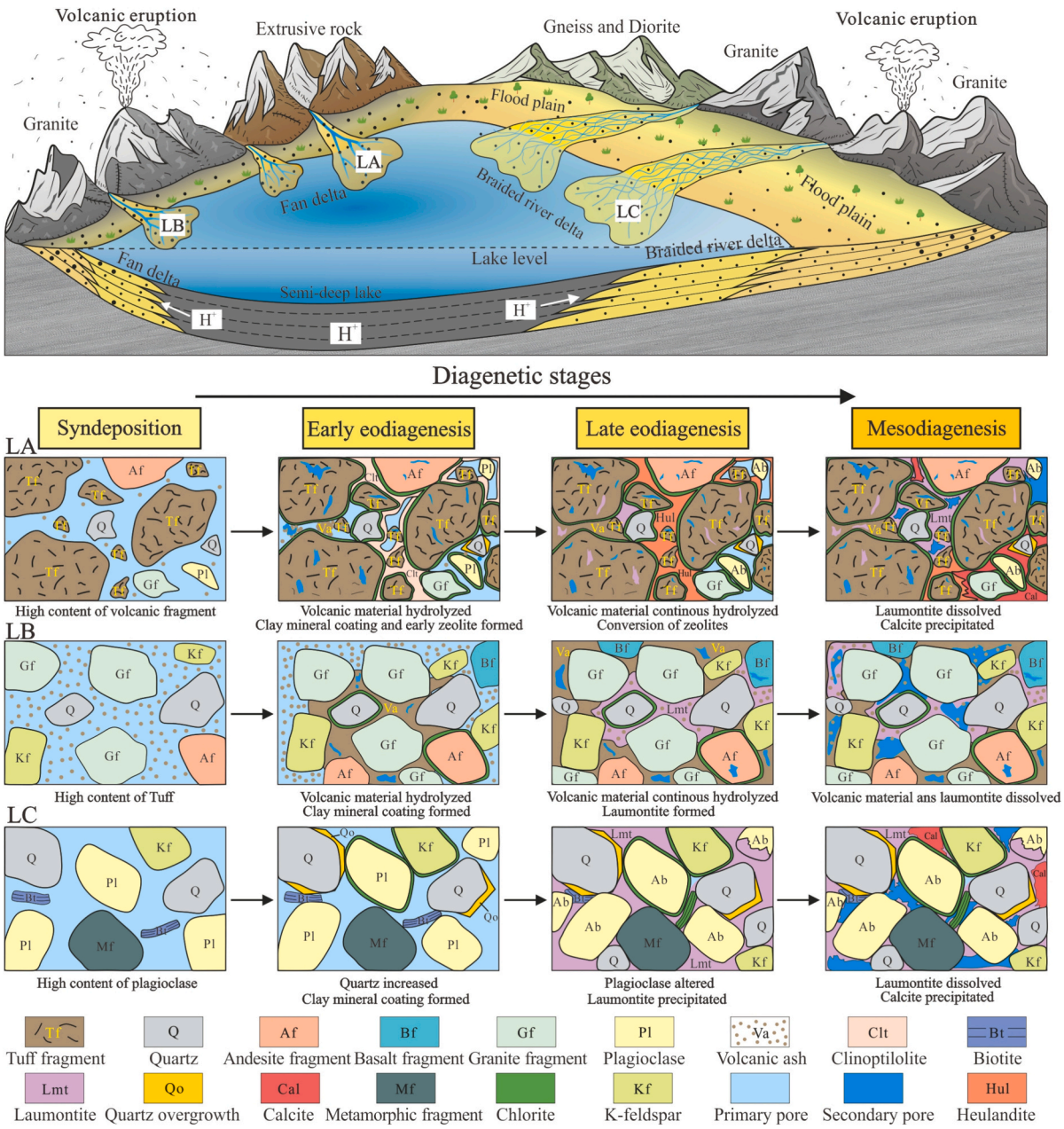

Fig. 11. The formation and evolution model of laumontite in the continental lacustrine sedimentary rocks of China.

kaolinite could react under specific conditions to form laumontite, following the reaction:

(Zen, 1961; Zhang, 1992).

$$CaCO_3 + Al_2Si_2O_5(OH)_4 + 2SiO_2 + 2H_2O = CaAl_2Si_4O_{12}{\cdot}4H_2O + CO_2 \quad (4)$$

However, this reaction mechanism has received little attention in the 21st century, primarily due to its high temperature requirement (>150 °C) (Huang et al., 2001) and the absence of direct, conclusive evidence supporting its occurrence.

Hydrothermal laumontite is rarely observed in sedimentary rocks across China but is well-documented in regions such as Japan and southern California, USA (Vincent and Ehlig, 1988; Iijima, 2001). Hydrothermal laumontite in sedimentary rocks is primarily distributed along fault zones and exhibits three characteristic modes of occurrence: fracture filling, intergranular cement, and replacement product. Its abundance generally decreases with increasing distance from the fractures. Early-stage hydrothermal laumontite initially fills pores and fractures, but subsequent tectonic activity may rupture the pre-existing laumontite veins. Additionally, well-crystallised laumontite formed through low-temperature hydrothermal processes has been reported at Sespe Hot Springs, California (Mcculloh et al., 1981). This variety typically occurs on rock surfaces or within fractures and is not associated with other zeolite minerals. Hydrothermal fluxes produced mineral phases that may contribut to the destruction of a potentially good reservoir by intense diagenesis (Caracciolo et al., 2014).

5.5. Formation and evolution model of laumontite

Three models describing the formation and evolution of laumontite in lacustrine sedimentary rocks of China have been summarised (Fig. 11). These correspond to:

1) (LA) sandstone and conglomerate rich in tuff clasts from the upper Wuerhe Formation in the Junggar Basin;
2) (LB) sandstone rich in intergranular volcanic ash from the Wenchang Formation in the Pearl River Mouth Basin;
3) (LC) sandstone rich in plagioclase from the Yanchang Formation in the Ordos Basin.

Model LA Junggar Basin: Intense volcanic activity during the early Permian resulted in the accumulation of abundant volcanic material within fan-delta sandstones and conglomerates of the Junggar Basin. By the time of the upper Wuerhe Formation deposition, volcanic activity had gradually declined, leading to a reduction in volcanic ash content between grains. However, the rock framework remained dominated by volcanic fragments, characterised by poor sorting and subangular to angular grain shapes. During early eodiagenesis, the hydrolysis of volcanic material released abundant alkaline ions and activated SiO_2, promoting the formation of clay mineral coatings, early hydrated zeolites, and quartz overgrowths. During late eodiagenesis, volcanic material continued to undergo hydrolysis, and clinoptilolite gradually transformed into heulandite with increasing temperature and pH. Throughout this process, the alteration of volcanic material could also directly supply the material required for laumontite formation. During mesodiagenesis, heulandite progressively transformed into laumontite. With increasing thermal maturity of organic matter, acidic fluids—such as organic acids—dissolved laumontite, feldspar, and volcanic material, resulting in the formation of secondary pores. Subsequently, the enrichment of alkaline ions elevated the pH of the pore fluids, leading to gradual saturation and precipitation of calcite and kaolinite, which later filled the secondary dissolution pores.

In this model, laumontite primarily occurs as patchy cement and as a replacement of volcanic fragments.

Model LB Pearl River Mouth Basin: Similarly influenced by multiphase volcanic activity, the sandstone of the Wenchang Formation in the Pearl River Mouth Basin contains a substantial amount of intergranular volcanic ash. Unlike other regions, the clastic components in this area are dominated by granite fragments, quartz, and feldspar, with only a low content of extrusive volcanic fragments. During early eodiagenesis, increasing burial depth led to the compaction and gradual hydrolysis of intergranular volcanic ash, resulting in the formation of minor clay mineral coatings. During late eodiagenesis, continued hydrolysis of volcanic material directly supplied the material required for laumontite formation, without evidence of other zeolites development. Mesodiagenesis was marked by intensified hydrolysis of volcanic material, resulting in the formation of numerous intergranular solution pores within volcanic ash. Simultaneously, acidic fluids entered and dissoluted the local laumontite, creating secondary pores. In this model, laumontite is primarily formed by replacing intergranular volcanic ash.

Model LC Ordos Basin: Although the Yanchang Formation experienced relatively intense volcanic activity, the deltaic sandstones exhibit high compositional maturity due to long-distance transport. Volcanic material content is low (<10 %), and clastic particles are predominantly quartz and feldspar. During early eodiagenesis, alteration of biotite and the migration of ions from adjacent mudstone layers led to the formation of chlorite coatings and a minor amount of quartz overgrowth in the sandstone. The albitisation of plagioclase progressed slowly at this stage. During late eodiagenesis, Laumontite rapidly precipitated between grains, occupying primary pores and replacing plagioclase. During mesodiagenesis, diagenetic reactions were similar to those in the LA model: a substantial amount of laumontite was dissolved by acidic fluids, after which calcite and illite precipitated and partially filled the resulting dissolution pores. In this model, laumontite primarily occurred in the form of continuous cement and replacement product of plagioclase.

6. Control factors of laumontite formation

Compared with analcime, laumontite exhibits a more restricted distribution in sedimentary rocks of continental lacustrine basins in China, reflecting its more stringent formation conditions (Zhu et al., 2020). The development of laumontite is controlled by multiple factors, including the sedimentary environment, lithology, temperature and pressure conditions, pore fluid chemistry, pH, and partial pressure of CO_2 (pCO_2).

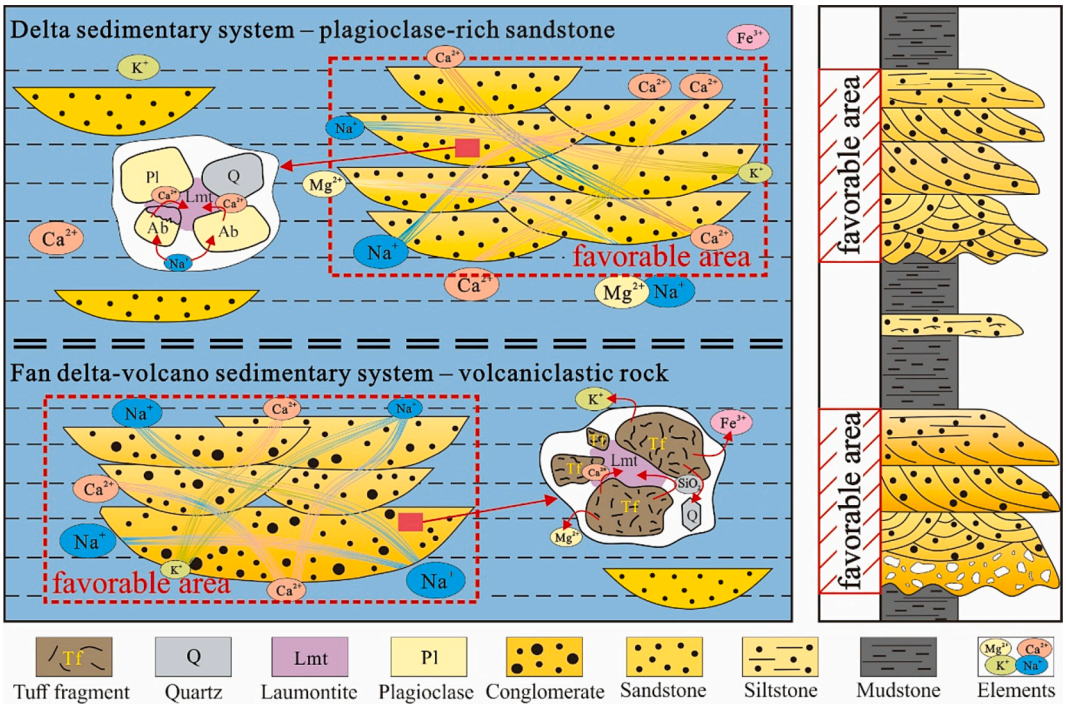

Fig. 12. Favourable sand body conditions for laumontite formation.

Table 5
Formation temperatures of laumontite in non-marine petroliferous basins in China and other typical globe basins.

Locality	Stratigraphy	Depositional environment	Depth/m	Occurrence	Genesis	Forming temperature	Associated authigenic phases	References
Huizhou Sag of Pearl River Mouth Basin, China	E_3w	Fan Delta	3000–4200	CPR	VZ	60–80 °C(I), 90–110 °C(II)	Quartz, Clay	Ma et al. (2023)
North Region of Songliao Basin, China	K_1q and K_1d	Fan Delta	2000–3200	PR	AV	110–143 °C	Albite, Quartz, Calcite, Clay	Wang et al. (2004)
Central Region of Sichuan Basin, China	J_2s	Delta	1500–3300	CPR	AVZ	60–70 °C(I), 70–100 °C(II)	Albite, Quartz, Calcite, Clay	Qing et al. (2020), Chen et al. (2024)
Western Region of Sichuan Basin, China	J_2s	Delta	900–3000	PR	AV	92–103.2 °C	Albite, Quartz, Calcite, Clay	Chen et al. (2024)
Northestern Region of Ordos Basin, China	T_3y^3	Braided River Delta	1000–2000	CPR	AV	65–85 °C(I), 105–120 °C(II)	Albite, Quartz, Calcite, Clay	Fu et al. (2010), Yang et al. (2002)
Southwestern Region of Ordos Basin, China	T_3y^{1-2}	Braided River Delta	1500–2500	CR	A	60–80 °C	Albite, Quartz, Calcite, Clay	Unpublished data source
Mahu Sag of Junggar Basin, China	P_2w	Fan Delta	3200–5000	CPFR	VZ	50–65 °C(I), 75–105 °C(II), >110 °C(III)	Heulandite, Albite, Quartz, Calcite, Clay	Yan (2019)
Shawan Sag of Junggar Basin, China	P_2w	Fan Delta	5000–7000	CPR	VZ	60–70 °C(I), 110–120 °C(II)	Heulandite, Albite, Quartz, Calcite, Clay	Zhang et al. (2024)
Zhongguai Uplift of Junggar Basin, China	P_1j	Fan Delta	3000–5500	CPR	VZ	68–85 °C	Heulandite, Albite, Quartz, Calcite, Clay	Li (2019)
Hokkaido, Honshu and Kyushu islands, Japan	N, E and K	Marine	2800–4500	PR	VZ	>140 °C	Heulandite, Albite, Quartz, Calcite, Clay	Aoyagi and Kazama (1980)
Santa Ynez Mountains, America	E	Turbidites, Shallow Marine and Fluvial	2500–6000	PFR	VZ	>110–173 °C	Heulandite, Albite, Quartz, Calcite, Clay	Helmold and van, (1984)
Central Coast Ranges east of San Francisco Bay, America	N	Turbidites, Marine	Outcrop	CPF	A	>100 °C	Heulandite, Albite, Quartz, Calcite, Clay	Murata and Whiteley (1973)
North Tejon oil fields, America	N	Turbidites, Marine	2500–3500	CPR	AVZ	<92 °C(Early), >94 °C(Late)	Heulandite, Albite, Quartz, Clay	Noh and Boles (1993)

The formation temperatures of laumontite in China were directly obtained from fluid inclusion measurements, while data from other areas were derived from strata temperature. C: continuous cement. P: patchy cement. F: fracture filling. R: replacement product. A. albitization of plagioclase. V. transformation of volcanic material. Z. transformation of early zeolite.

6.1. Sedimentary environment and rock types

In the sedimentary rocks of China, laumontite is commonly developed in the delta front of slightly saline lacustrine basins. Vertically stacked, multi-phase underwater distributary channels—characterised by strong hydrodynamic conditions, high compositional maturity, and good connectivity—are favourable for the efficient seepage and circulation of formation water (Hu et al., 2018; Fu et al., 2022; Wang et al., 2022a). This environment facilitates the effective seepage and exchange of formation water. In addition, the slightly saline sedimentary water is enriched in Ca, Na, and K, and the timely replenishment of these elements provides favourable conditions for the stable formation of laumontite (Fig. 12). In contrast, due to poor seepage conditions and inefficient ion exchange, mouth bars and isolated subaqueous distributary channel sand bodies are generally unfavourable for the formation of laumontite. Laumontite has also been found to develop in marine sedimentary environments worldwide, including coastal sands and turbidite fan sand bodies (Table 5).

Laumontite formation is primarily associated with two types of rocks:

1) Sandstones rich in volcanic material. Volcanic components typically contain abundant minerals that are unstable at low temperatures; their continuous hydrolysis releases abundant Ca^{2+}, K^{+}, Na^{+}, and Mg^{2+}, which are favourable for laumontite formation.
2) Sandstones rich in plagioclase, which can transform into laumontite under appropriate conditions due to the chemical and structural similarities.

6.2. Temperature and pressure

Thermodynamic calculations indicate that laumontite can form at temperatures above 36 °C under typical geological conditions (Huang et al., 2001). The minimum formation temperature decreases progressively with increasing pressure. Notably, temperature plays a significantly more dominant role than pressure in controlling the formation of laumontite (Sætre et al., 2018). The focus of this research is on discussing the impact of temperature. Fluid inclusion data of laumontite were collected and analysed from major basins in China, as well as from representative basins worldwide. It is worth noting that most studies on laumontite in Japan and the United States were conducted several decades ago, when analytical techniques were relatively limited. As a result, the formation temperatures of laumontite in these regions were often inferred from vitrinite reflectance (Ro) or the formation temperatures of associated minerals, which introduces a certain degree of uncertainty.

The analysis indicates that the formation temperature of laumontite is correlated with its occurrence, genesis, and timing of formation. For instance:

- Laumontite with continuous cementation typically forms earlier and at lower temperatures (60–80 °C)
- Patchy cementation develops slightly later at higher temperatures (>90 °C)
- No clear relationship has been identified between formation temperature and laumontite occurring as fracture filling or as a replacement product (Table 5)

Noh and Boles (1993) studied laumontite in volcaniclastic rocks from

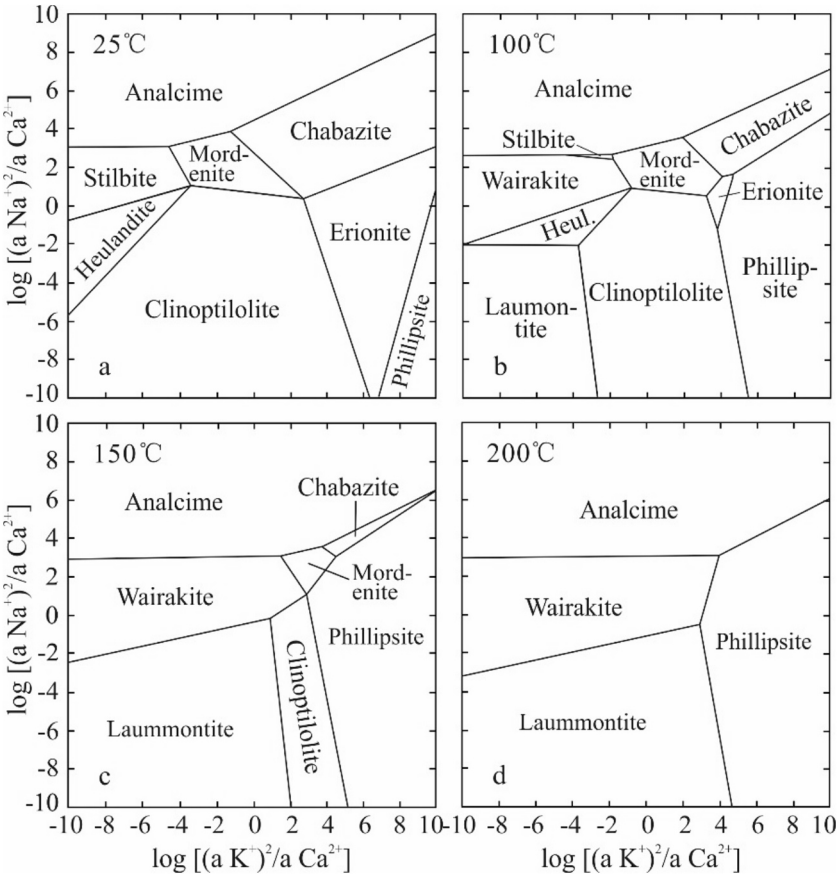

Fig. 13. Log [(a K^+)^2/a Ca^{2+}] versus log [(a Na^+)^2/a Ca^{2+}] diagrams for zeolite phases (Chipera and Apps, 2001). All calculated assuming an aqueous silica activity in equilibrium with quartz and at (a): 25 °C, (b): 100 °C, (c): 150 °C, (d): 200 °C.

the North Tejon oil fields and proposed that early-stage laumontite was transformed from heulandite at temperatures below 92 °C, while late-stage laumontite was associated with albitisation of plagioclase and formed at temperatures above 94 °C. Based on the integration of extensive data from China from the past two decades and comparison with global patterns of laumontite genesis, we propose the following:

- Laumontite formed through the albitisation of plagioclase or direct alteration of volcanic material can develop across a broad temperature range (60–140 °C)
- In contrast, laumontite derived from earlier zeolites such as heulandite tends to form at relatively higher temperatures, typically exceeding 90 °C (Iijima, 2001; Weibel et al., 2019)

Based on occurrence characteristics and fluid inclusion data, laumontite in major Chinese basins generally exhibits multi-stage formation characteristics. Early-formed laumontite may undergo two types of transformation during subsequent burial processes: it can either convert to prehnite under elevated temperatures or dissolve under the influence of acidic fluids.

6.3. Fluid chemical composition

The enrichment of Ca^{2+}, Al^{3+}, and SiO_2 in pore fluids promotes the formation of laumontite, which is primarily composed of these components. Ca^{2+} and SiO_2 can be supplied locally through the alteration of volcanic material, clay minerals, and plagioclase, or transported from more distant sources via fluid migration. In contrast, Al^{3+} is unlikely to be mobilised over long distances due to its low solubility, and therefore requires a local source (Hays and Boles, 1992).In addition, the presence of Na^+ lowers the equilibrium temperature of laumontite-forming reactions, thereby facilitating its formation (Iijima, 2001; Qi, 2013; Yang, 2014).

Chipera and Apps (2001) conducted thermodynamic simulations of zeolite equilibrium conditions in volcaniclastic rocks at varying temperatures. At the lowest temperature (25 °C), the stability diagrams resemble those calculated for diagenetically altered volcanic tuffs, whereas laumontite precipitation is thermodynamically unfavourable at this condition. Laumontite becomes stable in the more calcic fields of the phase diagram shown in Fig. 13. As temperature increases, the stability fields of laumontite, phillipsite, and wairakite progressively expand concurrent with contraction of other mineral domains, while the inhibitory effect of K^+ on laumontite stability gradually diminishes.

Sætre et al. (2018) explored the transformation of plagioclase to laumontite and suggested that the silica activity in formation waters must be close to or exceed quartz saturation in order to maintain laumontite stability. Fig. 14 illustrates the decreasing stability field for laumontite with temperature. Correspondingly, the minimum Ca^{2+} concentration required for laumontite saturation and precipitation decreases, while the minimum SiO_2 concentration increases. When the H^+ concentration rises, laumontite may dissolve and be replaced by other minerals such as kaolinite.

6.4. pH and pCO_2

A high pH and low pCO_2 are prerequisite conditions for the formation and continued stability of laumontite. When pH exceeds 9, the solubility of laumontite decreases, making it more likely to reach saturation and precipitate (Iijima, 2001; Bai et al., 2009). When pH decreases, laumontite becomes unstable and gradually dissolves, while the

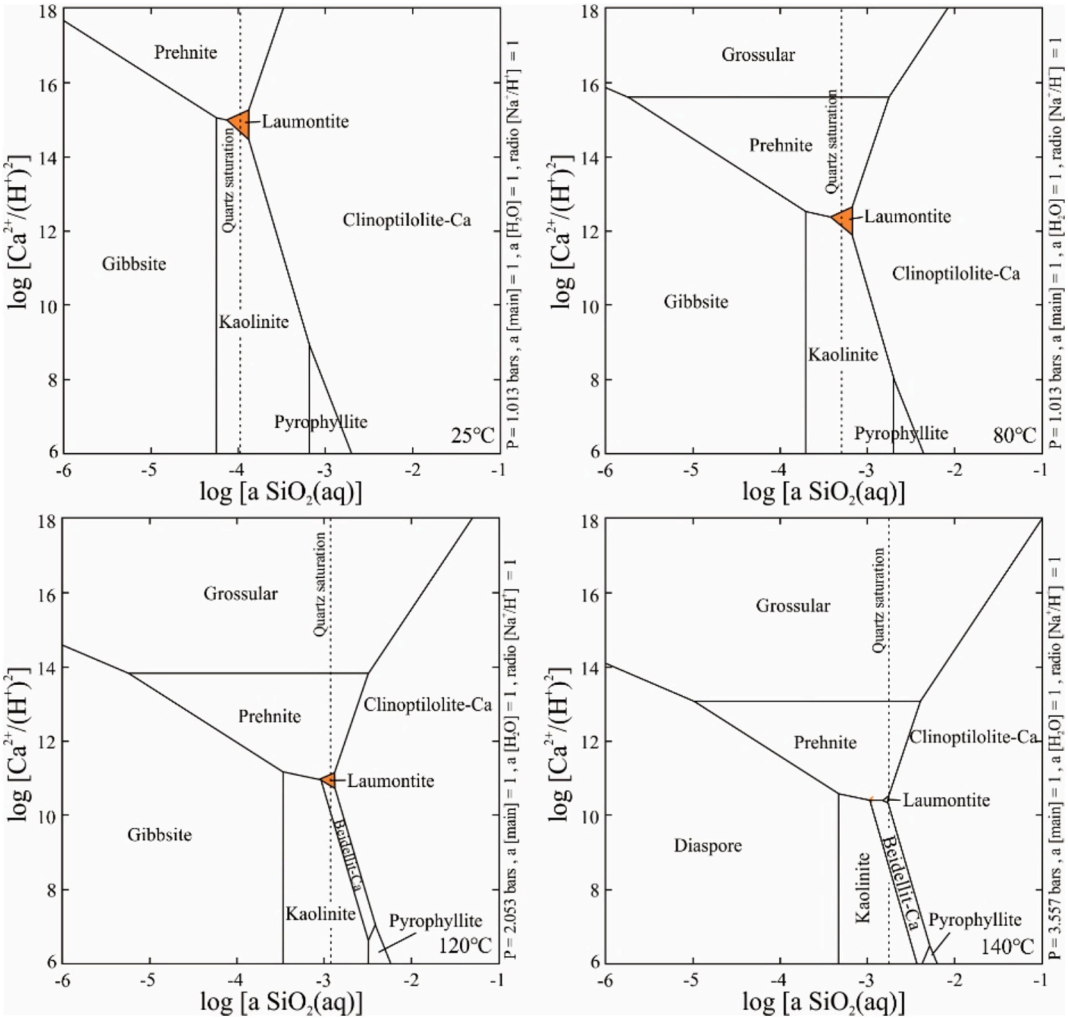

Fig. 14. Stability relationships among minerals at 25, 80, 120 and 140 °C (modified from Sætre et al., 2018). Dotted line shows silica saturation at quartz equilibrium.

diagenetic environment becomes more favourable for the precipitation of clay minerals (Tian et al., 2008). Due to the competitive relationship between laumontite and calcite for binding Ca^{2+}, high pCO_2 conditions promote the preferential precipitation of calcite from pore fluids, thereby immobilising Ca^{2+} (Helmold and Van, 1984; Huang et al., 2016). This, in turn, further inhibits the formation of laumontite.

7. Impact on hydrocarbon reservoir rocks

Early-stage laumontite precipitation occupies primary pores, leading to a reduction in reservoir porosity. Nevertheless, laumontite is highly sensitive to acidic fluids and can be readily dissolved, resulting in the formation of secondary pores—an important type of reservoir space in sandstones (Zhu et al., 2014b). The development of secondary pore zones associated with laumontite provides a foundation for the formation of high-yield oil and gas reservoirs (Wang et al., 2004). The following subsections focus on the effects of laumontite formation and dissolution on reservoir porosity, the selective dissolution of silicate minerals by acidic fluids, and the capacity of laumontite to adsorb natural gas.

7.1. Effect on primary pores

During eodiagenesis, laumontite produced as continuous and patchy cement, infilling the intergranular primary pores. Its replacement of plagioclase increases the solid volume by approximately 40 % (Savage et al., 1993). This not only significantly enhances the reservoir's resistance to compaction, making the loose rocks more stable, but also provides a material basis for the formation of later dissolution pores and the development of structural fractures. Additionally, some primary pores are preserved as intercrystalline pores within laumontite (Fig. 15a, b). In areas with limited dissolution, these intercrystalline pores play an important role in enhancing reservoir quality (Zhou et al., 2023).

7.2. Effect on secondary pores

As previously noted, laumontite is highly sensitive to the diagenetic environment and strongly influenced by acidic fluids. Laumontite with well-developed cleavage tends to dissolve rapidly along cleavage planes, whereas cleavage-poor laumontite dissolves progressively from the exterior inward. Under the influence of carbonic acid, laumontite can transform into kaolinite, calcite, and quartz according to the following reaction:

$$CaAl_2Si_4O_{12}\cdot 4H_2O + CO_2 = CaCO_3 + Al_2Si_2O_2(OH)_4 + 2SiO_2 + 2H_2O \quad (5)$$

The pCO_2 required for this reaction increases progressively with rising temperature (Fig. 16a).

Under the influence of organic acids, laumontite can transform into kaolinite and quartz:

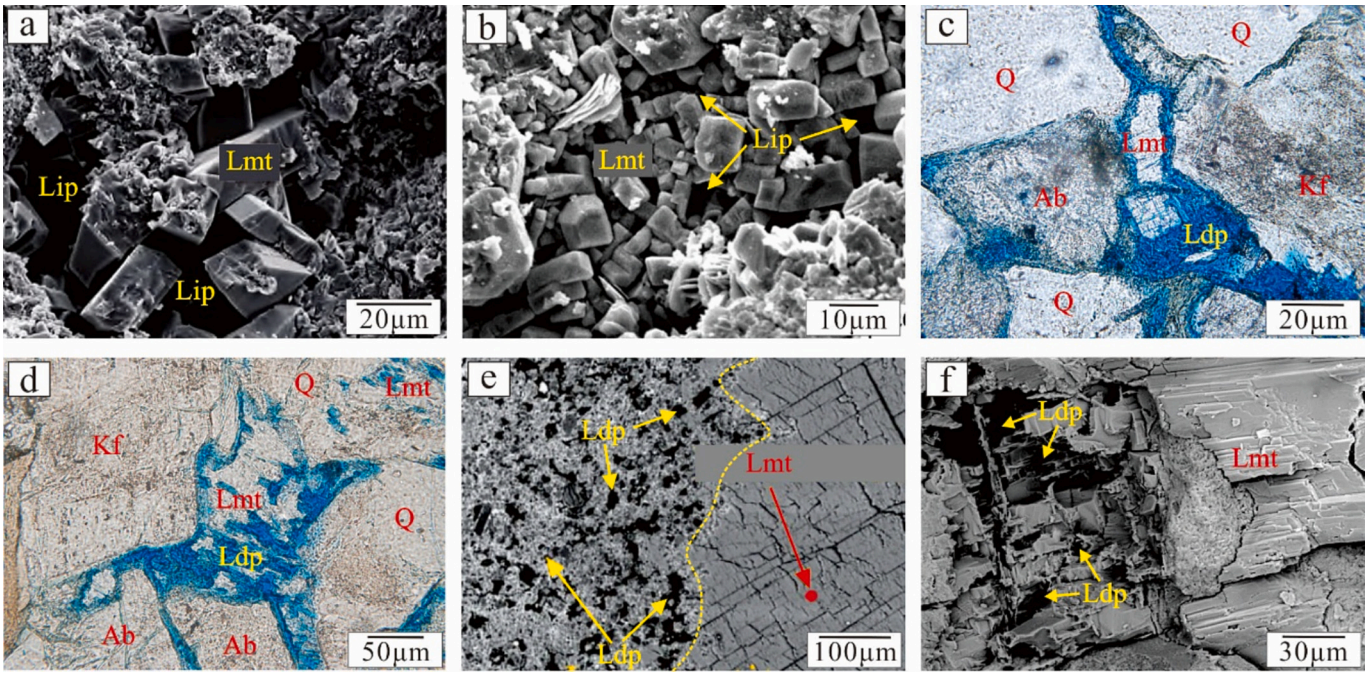

Fig. 15. Influence of laumontite-related intercrystalline pores (a-b) and dissolution pores (c-f) on hydrocarbon reservoir. (a) Well JL31, 3150.76 m, P_1j in Mahu region of Junggar Basin. (b) Well JL31, 3149.41 m, P_1j in Mahu region of Junggar Basin. (c) Well B420, 2426.9 m, T_3y^2 in Longdong region Ordos Basin. (d) Well L87, 1866.9 m, T_3y^1 in Longdong region Ordos Basin. (e) Well JL42, 2916 m, P_3w in Zhongguai uplift of Junggar Basin. (f) Well B420, 2426.9 m, T_3y^2 in Longdong region Ordos Basin. Lmt: laumontite; Lip: laumontite intercrystalline pore; Ldp: laumontite dissolved pore. a-b: from (Guo et al., 2022). e: from (Hong et al., 2022).

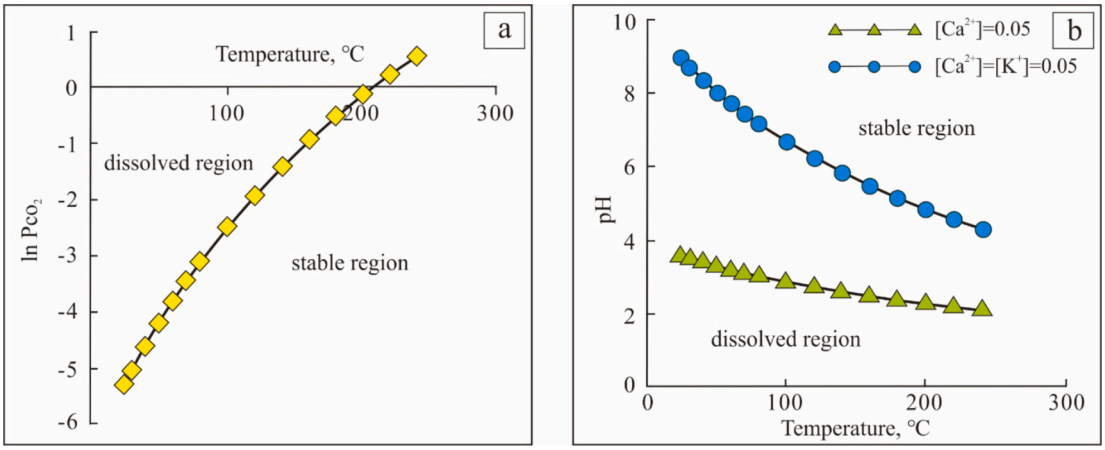

Fig. 16. Equilibrium states of laumontite dissolution reactions at 5 MPa under varying concentrations of (a) carbonic acid and (b) organic acids at different temperatures (modified from Qi, 2013).

$$CaAl_2Si_4O_{12}\cdot 4H_2O + 2H^+ = Al_2Si_2O_2(OH)_4 + 2SiO_2 + 3H_2O + Ca^{2+} \quad (6)$$

The required H^+ concentration increases progressively with rising temperature (Fig. 16b), while higher Ca^{2+} concentrations exert a pronounced inhibitory effect on this reaction. In a K-rich environment, laumontite dissolution by organic acids can lead to the formation of illite and quartz:

$$3CaAl_2Si_4O_{12}\cdot 4H_2O + 4H^+ + 2\,K^+ = 2KAl_3Si_3O_{10}(OH)_2 + 3Ca^{2+} + 6SiO_2 + 12H_2O \quad (7)$$

The presence of K^+ significantly enhances both the kinetics and overall rate of laumontite dissolution (Fig. 16b). Following the dissolution of laumontite by organic acids, released Ca^{2+} may react with CO_3^{2-}, leading to the precipitation of calcite (Helmold and van, 1984):

$$CaAl_2Si_4O_{12}\cdot 4H_2O + 6H^+ + CO_2 = CaCO_3 + 4SiO_2 + 7H_2O + 2Al^{3+} \quad (8)$$

The net solid volume changes for each reaction are: reaction (5) results in a solid volume reduction of approximately 28–30 %, reaction (6) by 10–12 %, and reaction (7) by about 33 % (Frost et al., 1982).

Thermodynamic calculations indicate that reaction (7) is most likely to occur spontaneously under burial conditions (Zhang et al., 2011). The above calculations are based on solid-phase transformations under closed-system conditions. In an open diagenetic environment, the dissolution products will be expelled with the fluids, resulting in a higher density of secondary pores (Fig. 15c-f). Consequently, reservoir porosity and permeability will experience a more significant increase (Yuan, 2015).

Extensive petrophysical data from Chinese laumontite-bearing sandstone reservoirs reveal that when laumontite content is below 10

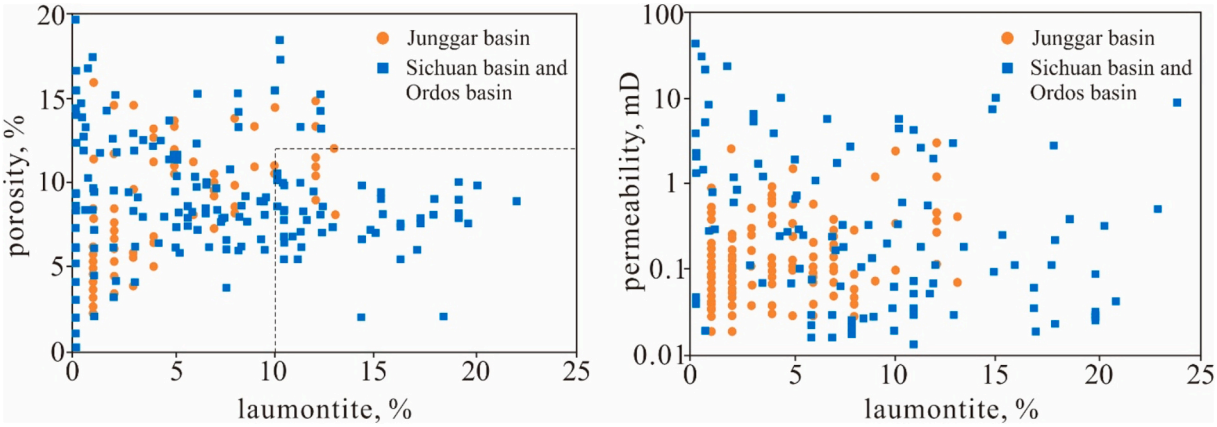

Fig. 17. Cross-plots of total porosity with laumontite content by volume. The data are from (Cai, 2016; Yan, 2021; Chen et al., 2024; Tan et al., 2024).

%, porosity exhibits considerable variability due to factors such as dissolution intensity, burial depth, and content of other cements. However, when laumontite content exceeds 10 %, reservoir porosity typically falls below 12 % (Fig. 17). This trend correlates well with observations by Bloch and Helmold (1995) in laumontite-bearing sandstones from the San Joaquin Basin, southern California, where they reported >10 % laumontite content corresponds with thin-section porosity <6 % (helium porosity <11 %). Notably, no strong correlation was observed between reservoir permeability and laumontite content.

Based on the preceding analysis, three principal factors govern the quality of laumontite-bearing reservoir rocks:

1) Depositional environment and lithology.
2) Acidic fluids derived from thermal degradation of kerogen.
3) Fluid migration pathways.

Studies from parts of North America indicate that laumontite formed during the late stage of diagenesis, or not subjected to acidic fluid alteration, shows a strong negative correlation with reservoir quality (Galloway, 1979; Crossey et al., 1984). These findings are consistent with Coffman's study in the Los Angeles Basin, which demonstrated that acidic fluid migration into shallow sandstones plays a critical role in early-stage laumontite dissolution (Iijima, 2001).

7.3. Selective dissolution under acidic conditions

Due to the high stability of clay minerals and the common precipitation of calcite following laumontite dissolution, this section focuses on the differential dissolution behaviour of organic acids on several typical silicate minerals (heulandite, laumontite, and feldspar). Heulandite and laumontite both belong to the zeolite group and share similar characteristics. However, heulandite has a higher Si/Al ratio and lower acid resistance, making it more susceptible to acidic dissolution. As a result, heulandite typically dissolves earlier than laumontite. The dissolution reactions of anorthite, albite, K-feldspar, and laumontite by organic acids can be represented by the following equations, respectively:

- $CaAl_2Si_2O_8 + 2H^+ + H_2O = Al_2Si_2O_5(OH)_4 + Ca^{2+}$ (9)
- $2NaAlSi_3O_8 + 2H^+ + H_2O = Al_2Si_2O_5(OH)_4 + 4SiO_2 + 2Na^+$ (10)
- $2KAlSi_3O_8 + 2H^+ + H_2O = Al_2Si_2O_5(OH)_4 + 4SiO_2 + 2\,K^+$ (11)
- $CaAl_2Si_4O_{12}{\cdot}4H_2O + 2H^+ = Al_2Si_2O_5(OH)_4 + 2SiO_2 + 3H_2O + Ca^{2+}$ (12)

Under standard conditions (25 °C, 1 bar), the equilibrium constants for the reactions are as follows:

$$\ln K\,(9) = 4.54 \times 10^{-2}, \ln K\,(10) = 3.39 \times 10^{-2}, \ln K\,(11) = 1.99 \times 10^{-2}, \ln K\,(12) = 3.13 \times 10^{-2}.$$

Based on these values, the relative sequence of mineral dissolution under identical temperature and H^+ conditions is: anorthite > albite > laumontite > K-feldspar (Qi, 2013). However, during the diagenetic process, laumontite is often dissolved by organic acids earlier than feldspars (Fig. 15c, d), as observed in the Yanchang Formation of the Ordos Basin and the Shaximiao Formation of the Sichuan Basin. This phenomenon may be attributed to the following factors:

1) By the time organic acids migrate into the reservoir rocks, most anorthite has already been altered to albite.
2) Although the equilibrium constants for the dissolution of albite and laumontite to kaolinite under acidic (H^+) conditions are similar, laumontite is more prone to dissolution due to its well-developed cleavage and larger crystal cavity volume.

When the scale and aggressiveness of acidic fluids exceed a certain threshold, the dissolution process becomes non-selective among these minerals.

7.4. Adsorption of natural gas

The unique connectivity of tetrahedra in laumontite results in the formation of numerous cavities and channels within its crystal structure. These voids are typically occupied by H_2O molecules. As temperature increases, laumontite gradually loses these H_2O molecules without disrupting its original crystal framework, creating cavities with a high specific surface area and strong physical adsorption capacity. Molecules with diameters smaller than the channel size can enter these cavities and be adsorbed.

Methane molecules (CH_4) have a diameter of approximately 3.8 Å, while the pore size of laumontite crystal ranges from 4.0 to 5.6 Å (Yang, 2014). This near-perfect fit allows CH_4 to be effectively confined within the crystal cavities. The uniform adsorption forces exerted by the surrounding pore walls create a superimposed potential field that strongly retains methane once it enters. Additionally, the cavities within the laumontite framework host exchangeable cations, while some framework oxygen atoms bear negative charges, giving rise to a strong local electrostatic field around the cations. The resulting electrostatic forces enhance the capacity of laumontite to adsorb methane molecules. In the Shaximiao Formation of the Sichuan Tianfu Gas Field, the development of laumontite has positively contributed to natural gas enrichment and accumulation.

8. Conclusion

1) The crystal habit of laumontite evolves from long prismatic to short prismatic with increasing temperature, and its aggregates commonly appear as columnar, fibrous, or radiating forms. In sedimentary rocks, laumontite occurs as continuous or patchy cement, fracture filling, and replacement product, with cementation and replacement being the most prevalent modes. Continuous cement forms prior to intense rock compaction, whereas patchy cement forms at a relatively later stage. Other occurrences of laumontite show no clear correlation with formation time.
2) Laumontite mainly forms during late eodiagenesis and early mesodiagenesis, whereas its dissolution primarily occurs in the early mesodiagenetic stage. During eodiagenesis, minerals such as I/S, chlorite, quartz, albite (derived from plagioclase), and heulandite commonly form. During mesodiagenesis, calcite, quartz, illite, kaolinite, albite (derived from plagioclase or analcime) and heulandite are typically present.
3) Laumontite is a Ca-rich zeolite mineral with the chemical formula $Ca[Al_2Si_4O_{12}]\cdot 4H_2O$. Its Si/Al ratio typically ranges from 2.00 to 2.20 showing no significant correlation with temperature or formation conditions. In sedimentary rocks of China, laumontite primarily forms through three genetic processes: plagioclase albitisation, alteration of volcanic material, and transformation of early-formed zeolites. Laumontite associated with volcanic alteration is the most widely distributed type in sedimentary basins across China. Under persistently alkaline conditions, laumontite may gradually transform into prehnite. In contrast, in diagenetic environments characterised by alternating alkaline-acidic-alkaline conditions, the multi-stage formation of laumontite is interrupted, and calcite precipitation is favoured instead.
4) Vertically stacked deltaic subaqueous distributary channel sands—composed of sandstones or conglomerates enriched in volcanic material or plagioclase—are favourable for laumontite formation under burial diagenetic conditions characterised by high pH, low pCO_2, and Ca^{2+} enrichment. Additionally, the presence of Na^+ can further promote the precipitation of laumontite. In China's sedimentary continental lacustrine basins, laumontite typically forms at temperatures ranging from 60 °C to 140 °C. When derived from the transformation of heulandite, laumontite generally forms at temperatures above 90 °C.
5) Early-formed laumontite fills primary pores, reducing reservoir quality but providing a material basis for subsequent dissolution. Under comparable conditions, the reaction in which laumontite is dissolved by organic acids and converted to illite and quartz in K^+-rich environments is the most thermodynamically favourable, resulting in the greatest reduction in solid volume during mineral transformation. Due to the combined influence of cleavage, crystal structure, and the equilibrium constants of dissolution reactions, laumontite is more readily dissolved by organic acids than K-feldspar and albite. The sedimentary environment, acidic fluids, and fluid migration pathways synergistically control the reservoir quality of laumontite-bearing sandstones. In addition, the well-developed channels and cavities within laumontite crystals facilitate the adsorption and storage of methane molecules.

Declaration of competing interest

The authors declare that they have no known competing financial interests or personal relationships that could have appeared to influence the work reported in this paper.

Acknowledgements

This research is supported by the National Natural Science Foundation of China (42272109, 41872102, 41202107). We are grateful to Editor Dr. Massimo Zecchin, the reviewer Dr. Luca Caracciolo and Dr. Salvatore Critelli for providing constructive comments that greatly enhanced the manuscript.

Data availability

Data will be made available on request.

References

Aoyagi, K., Kazama, T., 1980. Transformational changes of clay minerals, zeolites and silica minerals during diagenesis. Sedimentology 27 (2), 179–188.
Bai, Q.H., Liu, Y.Q., Fan, T.T., 2009. Genesis and distribution of laumontite in Yanhang Formation of Upper Triassic in Ordos Basin. Northwest. Geol. 42 (2), 100–107.
Baur, W.H., Joswig, W., Fursenko, B.A., Belitsky, L.A., 1997. Symmetry reduction of the aluminosilicate framework of LAU topology by ordering of exchangeable cations; the crystal structure of primary leonhardite with a primitive Bravais lattice. Eur. J. Mineral. 9 (6), 1173–1182.
Bloch, S., Helmold, K.P., 1995. Approaches to predicting reservoir quality in sandstones. Am. Assoc. Pet. Geol. Bull. 79 (01), 97–115.
Cai, Y., 2016. The Research on Sandy Conglomerate Reservoir Characteristics of Permian Jiamuhe Formation of the Southern Slope of Zhongguai Uplift. China University of Petroleum-Beijing, Beijing, China.
Caracciolo, L., Arribas, J., Ingersoll, R.V., Critelli, S., 2014. The diagenetic destruction of porosity in plutoniclastic petrofacies: The Miocene Diligencia and Eocene Maniobra formations, Orocopia Mountains, southern California, USA. In: Scott, R.A., Smyth, H. R., Morton, A.C., Richardson, N. (Eds.), Sediment Provenance Studies in Hydrocarbon Exploration and Production.
Chen, J., 2017. The Reservoir Characteristics of Yingcheng and Shahezi Formation in the Jinshan Gas Field, Lishu fault Depression. Chengdu University of Technology, Chengdu, Sichuan, China.
Chen, W.Z., Tian, J.C., Lu, Y.J., Liu, X.C., Wang, F., 2019a. Diagenesis and pore evolution of Chang 9 sandstone reservoir in Longdong area, Ordos Basin, China. J. Chengdu Univ. Technol. (Sci. Technol. Ed.) 46 (03), 342–353.
Chen, J.F., Yao, J.L., Mao, Z.G., Li, Q., Luo, A.X., Deng, X.Q., Shao, X.Z., 2019b. Sedimentary and diagenetic controls on reservoir quality of low-porosity and low-permeability sandstone reservoirs in Chang101, upper Triassic Yanhang Formation in the Shanbei area, Ordos Basin, China. Mar. Pet. Geol. 105, 204–221.
Chen, S.Y., Yang, Y.Q., Qiu, L.W., Wang, X.J., Habilaxim, E., 2024. Source of quartz cement and its impact on reservoir quality in Jurassic Shaximiao Formation in Central Sichuan Basin, China. Mar. Pet. Geol. 159 (1), 106543.
Chipera, S.J., Apps, J.A., 2001. Geochemical stability of natural zeolites. Rev. Mineral. Geochem. 45 (1), 117–161.
Civitelli, M., Critelli, S., Ingersoll, R.V., 2024. Interpreting post-depositional alterations in deep-marine sandstones: Butano Sandstone, Central California, USA. Mar. Pet. Geol. 163, 1–11.
Coffman, R.L., 1987. Laumontization and its relationship to carbonate cementation and dissolution within Santa Fe Springs Oil Field, Los Angeles Basin, California. AAPG Bull. 71 (5).
Coffman, R.L., 1988. Cementation in Los Angeles Basin: compositional and isotopic constraints. AAPG Bull. 72 (3), 17–19.
Coombs, D.S., 1954. The nature and alteration of some Triassic sediments from New Zealand. R. Soc. New Zealand 82, 65–109.
Crossey, L.J., Frost, B.R., Surdam, R.C., 1984. Secondary porosity in laumontite-bearing sandstones. In: McDonald, D.A., Surdam, R.C. (Eds.), Clastic Diagenesis.
Cui, H.N., 2007. Diagenesis and its influence on the pore characteristics of Wuerxun - Beier depressions in Hailaer Basin. Jilin University, Changchun, Jilin, China.
Fisher, R.V., Schmincke, H.-U., 1984. Alteration of volcanic glass. Pyroclastic Rocks 312–345.
Folk, R.L., 1968. Petrology of Sedimentary Rocks. Hemphill Publishing Co., Austin.
Frost, B., Surdam, R.C., Crossey, L.J., 1982. Secondary porosity in laumontite-bearing sandstones (abs.). Bull. Am. Assoc. Pet. Geol. 66, 569–570.
Fu, G.M., Dong, M.C., Zhang, Z.S., Sun, L., Pan, R., 2010. Formation process and distribution of Laumontite in Yanchang 3 reservoir of Fuxian Exploration Area in North Shaanxi Province and the controls of the high quality reservoirs. Earth Sci. 35 (01), 107–114.
Fu, Y., Luo, J.L., Shi, X.F., Cao, J.J., Mao, Q.R., Sheng, W.Y., 2022. Implications of lithofacies and diagenetic evolution for reservoir quality: a case study of the Upper Triassic Chang 6 tight sandstone, southeastern Ordos Basin, China. J. Pet. Sci. Eng. 218, 111051.
Galloway, W.E., 1979. Diagenetic controls of reservoir quality in arc-derived sandstones: Implications for petroleum exploration. In: Aspects of Diagenesis, 26. Society of Economic Paleontologists and Mineralogists Special, pp. 17–43.
Ghobarkar, H., Schäf, O., 1998. Hydrothermal synthesis of laumontite, a zeolite. Microporous Mesoporous Mater. 23 (1–2), 55–60.
Goodell, D.J., 1969. Laumontite. Rocks Miner. 44 (7), 509–510.
Guo, S.Q., 2018. Study on Diagenesis and Diagenetic Faceis of Yingcheng Formation in Longfengshan Sub-Sag, Songliao Basin. Chengdu University of Technology, Chengdu, Sichuan, China.
Guo, H., Ji, B.Q., Yang, S., Wang, R., Li, L.S., Zhang, S.Y., Zou, N.N., Shi, J.A., 2022. Formation of zeolite cements in Permian sandy conglomerate reservoir in the circum-Mahu sag, Junggar Basin and its petroleum geological significance. Acta Pet. Sin. 43 (03), 341–354.

Hall, A., Moss, S.J., 1997. The occurrence of laumontite in volcanic and volcaniclastic rocks from southern Sumatra. J. Asian Earth Sci. 15 (1), 55–59.
Hay, R.L., 1966. Zeolites and Zeolitic Reactions in Sedimentary Rocks, 1966. Geological Society of America, New York, pp. 1–85.
Hay, R.L., Sheppard, R.A., 2001. Occurrence of zeolites in sedimentary rocks: an overview. Rev. Mineral. Geochem. 45 (1), 217–234.
Hays, M.J., Boles, J.R., 1992. Volumetric relations between dissolved plagioclase and kaolinite in sandstones: Implications for mass transfer in the San Joaquin Basin, California. In: Origin, Diagenesis and Petrophysics of clay Minerals in Sandstones. Society for Sedimentary Geology, 47 (01), pp. 111–123.
He, Q., Yang, T., Cai, L.X., Ren, Q.Q., Dai, J., 2023. Porosity and permeability correction of laumontite-rich reservoirs in the first member of the Shaximiao Formation in the Central Sichuan Basin. Mar. Pet. Geol. 105 (2), 106115.
Helmold, K.P., 1979. Diagenesis of tertiary arkoses, Santa Ynez Mountains, Santa Barbara and Ventura Counties, California (abs). AAPG Bull. 63, 465.
Helmold, K.P., Van, P.C., 1984. Diagenetic mineralogy and controls on albitization and laumontite formation in Paleogene arkoses, Santa Ynez Mountains, California: part 2. aspects of porosity. Am. Assoc. Pet. Geol. Bull. 74 (03), 239–276.
Hong, H.L., Fang, Q., Wang, C.W., Gong, N.N., Zhao, L.L., 2017. Occurrence of palygorskite in late Oligocene in Linxia basin and its geological and climatic indicator, 42 (02), 161–172.
Hong, D.D., Cao, J., Guo, X.G., Bian, B.L., Liu, H.L., 2022. Diagenetic fluid controls chemical compositions of authigenic chlorite in clastic reservoirs. Mar. Pet. Geol. 137 (11), 105520.
Hou, Y.F., 2022. Study on Tight Sandstone Reservoir Evolution and Main Controlling Factors in the Lishu Fault Depression, Songnan. China University of Petroleum-Beijing, Beijing, China.
Hu, X., Ding, X.Q., Zhu, Y., Liu, X., 2018. Laumontite cement control mechanism of Yingcheng Formation of Longfengshan gas field. Fault-Block Oil & Gas Field 25 (02), 157–161.
Huang, S.J., Liu, J., Shen, L.C., Wu, W.H., 2001. Thermodynamic interpretation for the conditions of the formation of laumontite related to clastic diagenesis. Geol. Rev. 03, 301–308.
Huang, K.K., Zhong, Y.J., Liu, L., Hou, D.J., Hu, Z.J., 2016. Analysis of alteration process of plagioclase feldspar to laumontite during diagenesis by thermodynamic method. J. Chengdu Univ. Technol. (Sci. Technol. Ed.) 43 (04), 497–506.
Iijima, A., 1988. Chapter 3 Diagenetic transformations of minerals as exemplified by zeolites and silica minerals-a Japanese view. Dev. Sedimentol. 43, 147–211.
Iijima, A., 2001. Zeolites in petroleum and natural gas reservoirs. Rev. Mineral. Geochem. 45, 347–402.
Iijima, A., Utada, M., 1974. Present-Day Zeolitic Diagenesis of the Neogene Geosynclinal Deposits in the Niigata Oil Field, Japan. American Chemical Society, pp. 342–349.
Jin, Z.H., Yuan, G.H., Zhang, X.T., Cao, Y.C., Ding, L., Li, X.Y., Fu, X.H., 2023. Differences of tuffaceous components dissolution and their impact on physical properties in sandstone reservoirs: a case study on Paleogene Wenchang Formation in Huizhou-Lufeng area, Zhu I Depression, Pearl River Mouth Basin, China. Pet. Explor. Dev. 50 (1), 111–124.
Kaiser, W.R., 1984. Predicting reservoir quality and diagenetic history in the Frlo Formation (Oligocene) of Texas. In: Clastic Diagenesis, 37. AAPG Memoir, pp. 207–212.
Kaley, M.E., Hanson, R.F., 1955. Laumontite and leonhardite cement in Miocene sandstone from a well in San Joaquin Valley, California. Am. Mineral. 40, 923–925.
Koporulin, V.I., 2013. Formation of laumontite in sedimentary rocks: a case study of sedimentary sequences in Russia. Lithol. Miner. Resour. 48 (2), 122–137.
Kossovskaya, A.G., Shutov, V.D., 1965. Facies of regional epi-and metagenesis. Int. Geol. Rev. 7 (7), 1157–1167.
Kostov, I., 1967. Crystal habits of the zeolitic minerals. Krist. Tech. 2 (3), 305–318.
Lander, R.H., Bonnell, L.M., 2010. A model for fibrous illite nucleation and growth in sandstones. AAPG Bull. 94 (8), 1161–1187.
Li, J.F., 2019. Formation Mechanism and Reservoir Significance of Diagenetic Zeolites in Permian Glutenite Reservoirs at Zhongguai Area of the Northwestern Junggar Basin, NW China. Nanjing University, Nanjing, Jiangsu, China.
Li, B., Meng, Z.F., Li, X.B., Lu, H.X., Zheng, M., 2005. Diagenetic characteristics of the chang 6 oil-bearing interval of the upper Triassic in the Jin'an Oilfield, Ordos Basin. Acta Sedimentol. Sin. 04, 574–583.
Li, J., Zhang, W.J., Xiang, B.L., He, D., 2022. Characteristics of dissolved pores and dissolution mechanism of zeolite-rich reservoirs in the Wuerhe Formation in Mahu area, Junggar Basin. Energy Explor. Exploit. 40 (1), 421–441.
Lian, L.X., Yang, H.X., 2017. Impact of zeolite minerals on reservoir of Permian in Zhongguai Salient, the Northwestern of Junggar Basin. Geol. Rev. 63 (S1), 91–94.
Liang, H., Luo, Q.S., Kong, H.W., Fan, G.T., Ren, Z.W., Guo, K.C., 2011. Formation and distribution of zeolite in volcanic rock and its effect on reserviors in Santanghu Basin. Acta Sedimentol. Sin. 29 (03), 537–543.
Limarino, C.O., Giordano, S.R., Albertani, R.J.R., 2017. Diagenetic model of the Bajo Barreal formation (Cretaceous) in the southwestern flank of the Golfo de San Jorge Basin (Patagonia, Argentina). Mar. Pet. Geol. 88, 907–931.
Liu, Y.Q., 1996. The boundary between diagenesis and metamorphism a Discussion with reference to zeolite facies. Geol. Rev. 03, 215-222+290.
Liu, X.X., Zhang, S.N., Yang, P., Zhang, Y.M., He, H., 2017. Formation mechanism of deep high-quality reservoirs of Yingcheng Formation in Longfengshan area, Songliao Basin. Lithol. Reserv. 29 (02), 117–124.
Ma, B.B., Gao, J.C., Eriksson, K.A., Zhu, H.T., Liu, Q.H., Ping, X.Q., Zhang, Y., 2023. Diagenetic alterations in Eocene, deeply buried volcaniclastic sandstones with implications for reservoir quality in the Huizhou depression, Pearl River Mouth Basin, China. AAPG Bull. 107 (6), 929–955.
Mcculloh, T.H., Frizzell, V.A., Stewart, R.J., Ivan, B., 1981. Precipitation of Laumontite with Quartz, Thenardite, and Gypsum at Sespe Hot Springs, Western Transverse Ranges, California. Clay Clay Miner. 29, 353–364.
Meng, X.C., Chen, Y.G., Xie, Y.L., Guo, H.J., Luo, X., Dou, Y., Lu, H.G., Guo, Z.Y., 2020. Prediction criteria of laumontite-bearing sand-conglomerate reservoirs and optimization of potential oil and gas accumulation areas: taking P2w Formation in east slope of Mahu Sag as an example. J. Northeast Petrol. Univ. 44 (03), 1-13+141.
Murata, K.J., Whiteley, K.R., 1973. Zeolites in the Miocene Briones Sandstone and related formations of the central Coast Ranges, California, 1 (3), 225–265.
Nakajima, W., Tanaka, K., 1967. Zeolite-bearing tuffs from the Izumi Group in the central part of the Izumi Mountain Range, Southwest Japan, with reference to mordenite-bearing tuffs and laumontite tuffs. J. Geol. Soc. Jpn. 73 (5), 237–245.
Nan, Y., Liu, Y.Q., Zhou, D.W., Zhou, N.C., Jiao, X., Zhou, P., 2016. Characteristics and origin of amygdale and crack fillers in volcanic rock of Late Carboniferous in Santanghu basin, Xinjiang. Acta Sedimentol. Sin. 32 (06), 1901–1913.
Noh, J.H., Boles, J.R., 1993. Origin of zeolite cements in the Miocene sandstones, North Tejon oil fields, California. J. Sediment. Res. 63 (2), 248–260.
Ogihara, S., 1996. Diagenetic transformation of clinoptilolite to analcime in silicic tuffs of Hokkaido, Japan. Mineral. Deposita 31, 548–553.
Pan, H.Y., Tian, M., Zhao, Min, Liu, X.J., Hua, K.H., Lin, Q., 2015. Effect of SiO_2/Al_2O_3 ratios on catalytic performance of ZSM-5 for methanol to light olefins. Low-Carbon Chem. Chem. Eng. 40 (1), 9–12.
Qi, S.C., 2013. The Diagenesis of the Sandstone in Chang 8–10 Layer, Yanchang Formation, Longdong Region, Late Triassic of Ordos Basin and the Thermodynamics Behavior of Laumontite. Chengdu University of Technology, Cheng Du.
Qin, Z.J., Cao, Y.C., Mao, R., Zhang, H., Feng, C., 2023a. Characteristics and identification of zeolite-bearing tight sandy conglomerate reservoirs in Wuerhe Formation, Mahu Sag. Xinjiang Petrol. Geol. 44 (02), 136–143.
Qin, Z.J., Tang, Y., Chang, Q.S., 2023b. The characteristics and genetic mechanisms of the Upper Permian Shangwuerhe clastic reservoir in the eastern Junggar Basin, Northwest China. Front. Earth Sci. 10, 1057313.
Qing, Y.H., 2020. Formation Mechanism of Tight Oil Reservoirs in Liangshang Member and Shayi Member of Jurassic, Central Sichuan Basin. Chengdu University of Technology, Chengdu, Sichuan, China.
Qing, Y.H., Lu, Z.X., Zhao, F., Yang, J.J., Li, S., 2020. Formation mechanism of authigenic laumontites in tight sandstone of member 1 of the Middle Jurassic Shaximiao Formation in the Northeastern Central Sichuan Basin. Bull. Mineral. Petrol. Geochem. 39 (03), 536–547.
Rashchenko, S.V., Seryotkin, Y.V., Bakakin, V.V., 2012. An X-ray single crystal study of alkaline cations influence on laumontite hydration ability: I. Humidity-induced hydration of Na, K-rich laumontite. Microporous Mesoporous Mater. 151 (07), 93–98.
Remy, R.R., 1994. Porosity reduction and major controls on diagenesis of Cretaceous-Paleocene volcaniclastic and arkosic sandstone, Middle Park Basin, Colorado, 64 (4a), 797–806.
Sætre, C., Hellevang, H., Dennehy, C., 2018. A diagenetic study of intrabasaltic siliciclastic sandstones from the Rosebank field. Mar. Pet. Geol. 98, 335–355.
Savage, D., Cave, M.R., Haigh, D., Milodowski, A.E., Young, M.E., 1993. The reaction kinetics of laumontite under hydrothermal conditions. Eur. J. Mineral. 5 (3), 523–535.
Shan, X., Dou, Y., Liu, C.W., Pan, J., Guo, G.H., Peng, B., Li, K., 2023. Characteristics and controlling factors of deep buried tight conglomerate: a case study from the Permian Upper Urho Formation of Fukang Sag, Junggar Basin. Acta Sedimentol. Sin. 11 (3), 1–18.
Stewart, R.J., Mcculloh, T.H., 1977. Widespread occurrence of laumontite in late Mesozoic and Tertiary basins of Pacific margin. Am. Assoc. Pet. Geol. Bull. 61 (02), 1392–1393.
Sun, Y.S., Cao, Z.Q., 1991. Characteristics and distribution of zeolite group minerals in Karamay Oilfields. Xinjiang Petrol. Geol. 12 (3), 253–261.
Sun, J., You, X.C., Zhang, Q., Xue, J.J., Chang, Q.S., 2023. Development characteristics and genesis of deep tight conglomerate reservoirs of Mahu area in Junggar Basin. Nat. Gas Geosci. 34 (02), 240–252.
Tan, X.F., Jiang, W., Luo, L., Gluyas, J., Liu, J.P., Qu, X.J., Wang, J., Gao, X.B., Zhang, W., Chen, L., 2024. Variations of sedimentary environment under cyclical aridification and impacts on eodiagenesis of tight sandstones from the late Middle Jurassic Shaximiao Formation in Central Sichuan Basin. Mar. Pet. Geol. 161 (8), 106699.
Tian, J.F., Chen, Z.L., Yang, Y.Y., 2008. Protection mechanism of authigenic chlorite on sandstone reservoir pores. Bull. Geol. Sci. Technol. 04, 49–54.
Utada, M., 1965. Zonal distribution of authigenic zeolites in the Tertiary pyroclastic rocks in Mogami district, Yamagata Prefecture. Coll. Gen. Educ. Univ. Tokyo 15 (2), 173–216.
Vavra, C.L., 1989. Mineral reactions and controls on zeolite-facies alteration in sandstone of the central Transantarctic Mountains, Antarctica. J. Sediment. Res. 59 (5), 688–703.
Vincent, M.W., Ehlig, P.L., 1988. Laumontite mineralization in rocks exposed north of San Andreas Fault at Cajon Pass, southern California. Adv. Earth Space Sci. 15 (9), 977–980.
Wang, C., Shao, H.M., Hong, S.X., Qi, X.J., 2004. Formation and evolution of laumontite and relationship between oil and gas in the clastic rock of the deep strata of the North Songliao Basin. Bull. Mineral. Petrol. Geochem. 03, 213–218.
Wang, Y.Z., Lin, M.R., Xi, K.L., Cao, Y.C., Wang, J., Yuan, G.H., Kashif, M., Song, M.S., 2018. Characteristics and origin of the major authigenic minerals and their impacts on reservoir quality in the Permian Wutonggou Formation of Fukang Sag, Junggar Basin, western China. Mar. Pet. Geol. 97, 241–259.
Wang, L., Deng, X.Q., Chu, M.J., Zhang, Z.Y., Ren, Z.C., Liu, G.L., Zhang, W.J., Qi, Y.L., 2022a. Formation and distribution of laumontite in sedimentary sequences and their

exploration significance-a case study on the Middle-Upper Triassic Yanchang Formation in Ordos Basin. Geol. Rev. 68 (06), 2188–2206.
Wang, X.J., Hong, H.T., Wu, C.J., Liu, M., Guan, X., 2022b. Characteristics and Formation mechanisms of tight sandstone reservoirs in Jurassic Shaximiao Formation, Central of Sichuan Basin. J. Jilin Univ. (Earth Sci. Ed.) 52 (04), 037–1051.
Weibel, R., Olivarius, M., Jakobsen, F.C., Whitehouse, M., Larsen, M., Midtgaard, H., Nielsen, K., 2019. Thermogenetic degradation of early zeolite cement: an important process for generating anomalously high porosity and permeability in deeply buried sandstone reservoirs? Mar. Pet. Geol. 103, 620–645.
Winkler, H.G.F., 1979. Petro Genesis of Metamorphic Rocks, 10 (02). Springer Verlag, New York, pp. 1–2.
Wopfner, H., Markwort, S., Semkiwa, P., 1991. Early diagenetic laumontite in the Lower Triassic Manda Beds of the Ruhuhu Basin, Southern Tanzania. J. Sediment. Petrol. 61 (01), 65–72.
Xiao, Y., Wang, J.X., Xiao, B.Y., Cao, J.X., Li, T.L., Zhong, Z.Y., Fan, C.H., 2023. Characteristics and main controlling factors of tight sandstone reservoir in the first member of Jurassic Shaximiao Formation in Tianfu gas-bearing area, Sichuan Basin. Nat. Gas Geosci. 34 (11), 1916–1926.
Xing, S.Q., Zhang, S.G., 1982. Originating conditions of autogenetic laumontite in sandstones and its geological significance. Petrol. Geol. Oilfield Dev. Daqing 02, 79–86.
Yan, Q., 2019. Genesis of Zeolite and its Reservoir Significance of Lower Urhe Formation in Mahu Depression. University of Petroleum-Beijing, Beijing, China.
Yan, M., 2021. The Characteristics of Chang 6_2 and Chang 6_3 Reservoirs and its Oil Control Infoguyuan, Ordos Basin. Xi'an ShiYou Unersity, Xi'an, Shannxi, China.
Yanagimoto, Y., Iijima, A., 2006. Hydrothermal laumontization and microfracture formation in reservoir rocks at the Yufutsu Field, Hokkaido, Northern Japan. J. Pet. Geol. 26 (03), 351–372.
Yang, M., 2014. Sandstone Petrography and the Cause of Laumontite Cements in Yanchang 9 Layer of Ordos Basin. Chengdu University of Technology, Chengdu, Sichuan, China.
Yang, X.P., Qiu, Y.N., 2002. Formation process and distribution of laumontite in Yanchang Formation (Upper Triassic) of Ordos Basin. Acta Sedimentol. Sin. 20 (04), 628–632.
Yang, B.X., Lin, Z.Q., Gu, S.X., 1991. Diagenesis of laumontite-bearing sandstones in lower part of lower cretaceous North Songliao Basin. Oil Gas Geol. 01, 1-9+95-96.
Yang, G.F., Zhuo, S.G., Teng, Y.H., Niu, B., E, J.J., 2002. Characteristics of diagenetic secondary mineralism the sandstone of the Songliao Basin. Pet. Geol. Exp. 06, 517–522.
Yang, G.F., Zhuo, S.G., Niu, B., 2003. Albitization of detrital feldspar in cretaceous sandstones from the Songliao Basin. Geol. Rev. 02, 155-161+228.
Yang, S.Y., Liu, L.F., Xu, Z.J., Shao, M.L., Jia, K.X., Dou, W.C., Wan, Q.Q., Liu, X.Q., Song, Y.P., Guo, C.Y., 2017. Diagenesis and diagenetic facies of the lower Cretaceous Yingcheng formation sandstones in the Dehui fault depression in the southern Songliao basin, China. J. Northeast Petrol. Univ. 41 (03), 52-62+72+8-9.
Yoshimura, T., 1961. Zeolites in the Miocene pyroclastic rocks in the Oshima-Fukushima district, Southwestern Hokkaido. J. Geol. Soc. Jpn. 67 (793), 578–583.
Yu, Z.F., Chen, R.H., Zhao, X.Q., Sun, F.X., 2012a. Types and Succession of pyroclastic rocks diagenesis in Lower Cretaceous of Wuerxun and Bei'er Depression in Hailaer Basin. Earth Sci. 37 (04), 851–859.
Yu, M., Liu, L., Zhang, J.G., Zhao, S., Meng, F.Q., Zhou, B., 2012b. The authigenetic mineral association succession of laumontite-bearing sandstones and the characteristic of reservoir space in the Tongfosi-Dalazi Formation of Lower Cretaceous, Yanji Basin. J. Jilin Univ. (Earth Sci. Ed.) 42 (S3), 14–24.
Yu, J., Zhang, K.H., Lin, C.M., Zhang, X., Zhang, N., 2016. Diagenesis characteristics of Permian reservoir in Chaiwopu Depression, Junggar Basin. Lithol. Reserv. 28 (03), 95–104.
Yuan, G.H., 2015. Genetic Mechanism of Dissolution of Feldspars and Carbonate Minerals during Diagenesis and its Impact on Reservoir Poroperm. China University of Petroleum (East China), Qingdao, China.
Yuan, Z., Zheng, Y.Z., Yuan, H.L., Yang, X.Y., Li, W.H., 2020. Study on the characteristics and diagenesis model of laumontite cement in Yanchang Formation in the southeastern margin of Ordos Basin. J. Northwest Univ. (Nat. Sci. Ed.) 50 (01), 124–134.
Zen, E.M., 1961. The zeolite facies; an interpretation. Am. J. Sci. 259, 401–409.
Zhang, L.F., 1992. Burial metamorphism of the basin in Northern Shaanxi. Acta Geol. Sin. 66 (04), 339-349+393-394.
Zhang, X.H., Huang, S.J., Lan, Y.F., Huang, K.K., Liang, R., 2011. Thermodynamic calculation of laumontite dissolution and its geologic significance. Lithol. Reserv. 23 (02), 64–69.
Zhang, Y.M., Ding, X.Q., Yang, P., Liu, Y., Jiang, Q., Zhang, S.N., 2016. Reservoir formation mechanism analysis and deep high-quality reservoir prediction in Yingcheng Formation in Longfengshan area of Songliao Basin, China. Petroleum 2 (4), 334–343.
Zhang, Y., Ma, B.B., Jiang, S., Wang, H., Yan, D., Lu, Y.C., Ye, J.R., 2024. Formation mechanisms of anomalously high reservoir quality in deep-buried volcaniclastic sandstones, central Junggar basin, northwestern China. Mar. Pet. Geol. 163, 106772.
Zhao, C.Y., Shi, X., Liao, W., Yan, L.H., Dai, C.X., Li, X.T., Shi, Y.M., Zheng, H.X., 2023. Formation and erosion of zeolites in conglomerate reservoirs impact on physical properties: an example of a conglomerate gas reservoir of Lower Permian Jiamuhe Formation in Middle Abduction Bulge on Northwest Margin of Junggar Basin. Acta Sci. Nat. Univ. Pekin. 59 (05), 782–792.
Zhi, D.M., Kang, X., Qin, Z.J., Tang, Y., Cao, J., Hu, R., 2022. Fluid-rock interactions and porosity genesis in deep clastic reservoirs: a perspective of differential oil charge intensity. Mar. Pet. Geol. 137 (5), 105508.
Zhou, X.N., 2019. Diagenesis and Pore Evolution of Chang 6 Reservoir in Jiyuan Area. Northeast Petroleum University, Daqing, Heilongjiang, China.
Zhou, J.J., Wu, H.G., Wang, J., Hu, G., Zhang, Y.F., Feng, J.L., Li, Y.L., 2023. Quantitative assessment of the effects of zeolite alteration processes on deep clastic reservoirs–a case study of the Jiamuhe Formation in the Shawan Sag, Junggar Basin, China. Mar. Pet. Geol. 154 (8), 106286.
Zhu, G.H., 1985. Formation of limonitic sand bodies with secondary porosity and their relationship with hydrocarbons. Acta Pet. Sin. 6 (01), 1–8.
Zhu, S.F., Zhu, X.M., Wang, X.L., Liu, Z.Y., 2012. Zeolite diagenesis and its control on petroleum reservoir quality of Permian in northwestern margin of Junggar Basin, China. Sci. China Earth Sci. 55 (3), 386–396.
Zhu, S.F., Zhu, X.M., Wu, D., Liu, Y.H., Li, P.P., Jiang, S.X., Liu, X.C., 2014a. Alteration of volcanic and its controlling factors in the Lower Permian reservoirs at northwestern margin of Junggar Basin. Oil Gas Geol. 35 (01), 77–85.
Zhu, S.F., Zhu, X.M., Liu, X.C., Li, C., Wang, X.X., Tan, M.X., Geng, M.Y., Li, Y.P., 2014b. Alteration products of volcanic materials and their influence on reservoir space in hydrocarbon reservoirs: evidence from Lower Permian strata in Ke-Xia region, Junggar Basin, 35 (02), 276–285.
Zhu, S.F., Jia, Y., Cui, H., Dowey, P.J., Taylor, K.G., Zhu, X.M., Liang, T., 2019. Alteration and burial dolomitization of fine-grained, intermediate volcaniclastic rocks under saline-alkaline conditions: Bayindulan Sag in the Er'Lian Basin, China. Mar. Pet. Geol. 110, 621–637.
Zhu, S.F., Cui, H., Jia, Y., Zhu, X.M., Tong, H., Ma, L.C., 2020. Occurrence, composition, and origin of analcime in sedimentary rocks of non-marine petroliferous basins in China. Mar. Pet. Geol. 113, 104–164.